Article

Cell Metabolism

Modulation of Autophagy by BDNF Underlies Synaptic Plasticity

Graphical Abstract

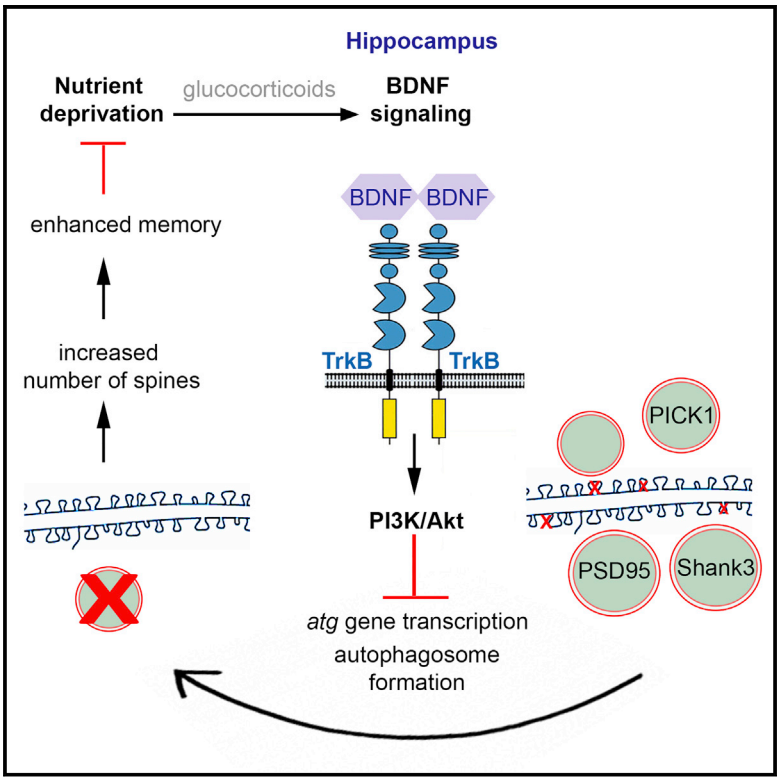

Authors

Vassiliki Nikoletopoulou, Kyriaki Sidiropoulou, Emmanouela Kallergi, Yannis Dalezios, Nektarios Tavernarakis

Correspondence

n.vassiliki@imbb.forth.gr (V.N.), tavernarakis@imbb.forth.gr (N.T.)

In Brief

Nikoletopoulou and colleagues find that specific brain regions regulate autophagy differentially in response to nutritional stress. They demonstrate that fasting suppresses autophagy in regions of the mouse forebrain, thereby promoting synaptic remodeling and memory through a BDNF-regulated mechanism.

Highlights

- Autophagy is differentially regulated by fasting in different brain regions
- BDNF signaling suppresses autophagy in the forebrain of adult mice
- BDNF ablation in the neural lineage causes uncontrolled increase in autophagy
- Increased autophagy mediates the synaptic defects caused by BDNF deficiency

Nikoletopoulou et al., 2017, Cell Metabolism *26*, 230–242
July 5, 2017 © 2017 Elsevier Inc.
http://dx.doi.org/10.1016/j.cmet.2017.06.005

CellPress

Cell Metabolism
Article

Modulation of Autophagy by BDNF Underlies Synaptic Plasticity

Vassiliki Nikoletopoulou,[1,*] Kyriaki Sidiropoulou,[2] Emmanouela Kallergi,[1] Yannis Dalezios,[3] and Nektarios Tavernarakis[1,3,4,*]

[1]Institute of Molecular Biology and Biotechnology, Foundation for Research and Technology – Hellas, Nikolaou Plastira 100, Heraklion 70013, Crete, Greece

[2]Department of Biology, University of Crete, Heraklion 70013, Crete, Greece

[3]Department of Basic Sciences, Faculty of Medicine, University of Crete, Heraklion 71110, Crete, Greece

[4]Lead Contact

*Correspondence: n.vassiliki@imbb.forth.gr (V.N.), tavernarakis@imbb.forth.gr (N.T.)

http://dx.doi.org/10.1016/j.cmet.2017.06.005

SUMMARY

Autophagy is crucial for neuronal integrity. Loss of key autophagic components leads to progressive neurodegeneration and structural defects in pre- and postsynaptic morphologies. However, the molecular mechanisms regulating autophagy in the brain remain elusive. Similarly, while it is widely accepted that protein turnover is required for synaptic plasticity, the contribution of autophagy to the degradation of synaptic proteins is unknown. Here, we report that BDNF signaling via the tropomyosin receptor kinase B (TrkB) and the phosphatidylinositol-3′ kinase (PI3K)/Akt pathway suppresses autophagy *in vivo*. In addition, we demonstrate that suppression of autophagy is required for BDNF-induced synaptic plasticity and for memory enhancement under conditions of nutritional stress. Finally, we identify three key remodelers of postsynaptic densities as cargo of autophagy. Our results establish autophagy as a pivotal component of BDNF signaling, which is essential for BDNF-induced synaptic plasticity. This molecular mechanism underlies behavioral adaptations that increase fitness in times of scarcity.

INTRODUCTION

The highly specialized neurons of the vertebrate brain depend on catabolic processes, not only to eliminate waste, but also to adapt to variations in nutrient availability and to promote cellular plasticity, ultimately culminating in changes in behavior and physiology.

Appreciation of the role of autophagy in brain function continues to expand, as emerging evidence indicates that autophagy-mediated degradation is essential for neuronal integrity. On the one hand, under conditions of stress, excessive autophagy has been shown to play a deleterious role in neurons, promoting damage and loss. For example, inhibition of macroautophagy during excitotoxic stress can be protective and potentially promotes neuronal recovery (Dong et al., 2012; Koike et al., 2008; Yue et al., 2002). On the other hand, genetic studies with conditional deletion of key autophagy genes, such as *atg5* or *atg7*, in the neural lineage indicate that defects in baseline autophagy culminate in progressive neurodegeneration (Hara et al., 2006; Komatsu et al., 2006; Liang et al., 2010).

In addition to serving housekeeping functions, neuronal autophagy has also been implicated in synaptic function. In the presynaptic sites, recent work demonstrated that chronic autophagy deficiency in dopaminergic neurons results in increased size of axon profiles, increased dopamine release, and more rapid presynaptic recovery (Hernandez et al., 2012). On the postsynaptic side, autophagy was also shown to have a critical role in the elimination of dendritic spines in the cortex during the period of developmental pruning (Tang et al., 2014).

These findings suggest that autophagy has a role in modulating synaptic organization and morphogenesis, highly dynamic processes that underlie the fascinating plasticity of neuronal function. Despite this, the molecular mechanisms that regulate autophagy in the brain remain unknown. Similarly, while it is widely accepted that protein turnover is required for synaptic plasticity (Alvarez-Castelao and Schuman, 2015), the contribution of autophagy to the degradation of synaptic proteins is still elusive.

Here we report that BDNF signaling suppresses autophagy in the adult brain by transcriptionally downregulating key components of the autophagic machinery. Therefore, BDNF is crucial for maintaining the baseline autophagic activity in the brain and BDNF deficiency causes an uncontrolled rise in autophagic degradation. Moreover, we reveal that increased autophagy mediates the synaptic defects caused by BDNF deficiency and is a crucial component required for BDNF-induced synaptic plasticity. We also provide significant insight into how autophagy may regulate synapses by directly degrading key synaptic protein substrates.

RESULTS

Regulation of Autophagy in the Brain Is Region Specific

We examined the spatial regulation of autophagy in the adult brain in a paradigm of fasting known to increase autophagy across peripheral tissues (Mizushima et al., 2004). To circumvent the caveats associated with the use of mice overexpressing a

CrossMark

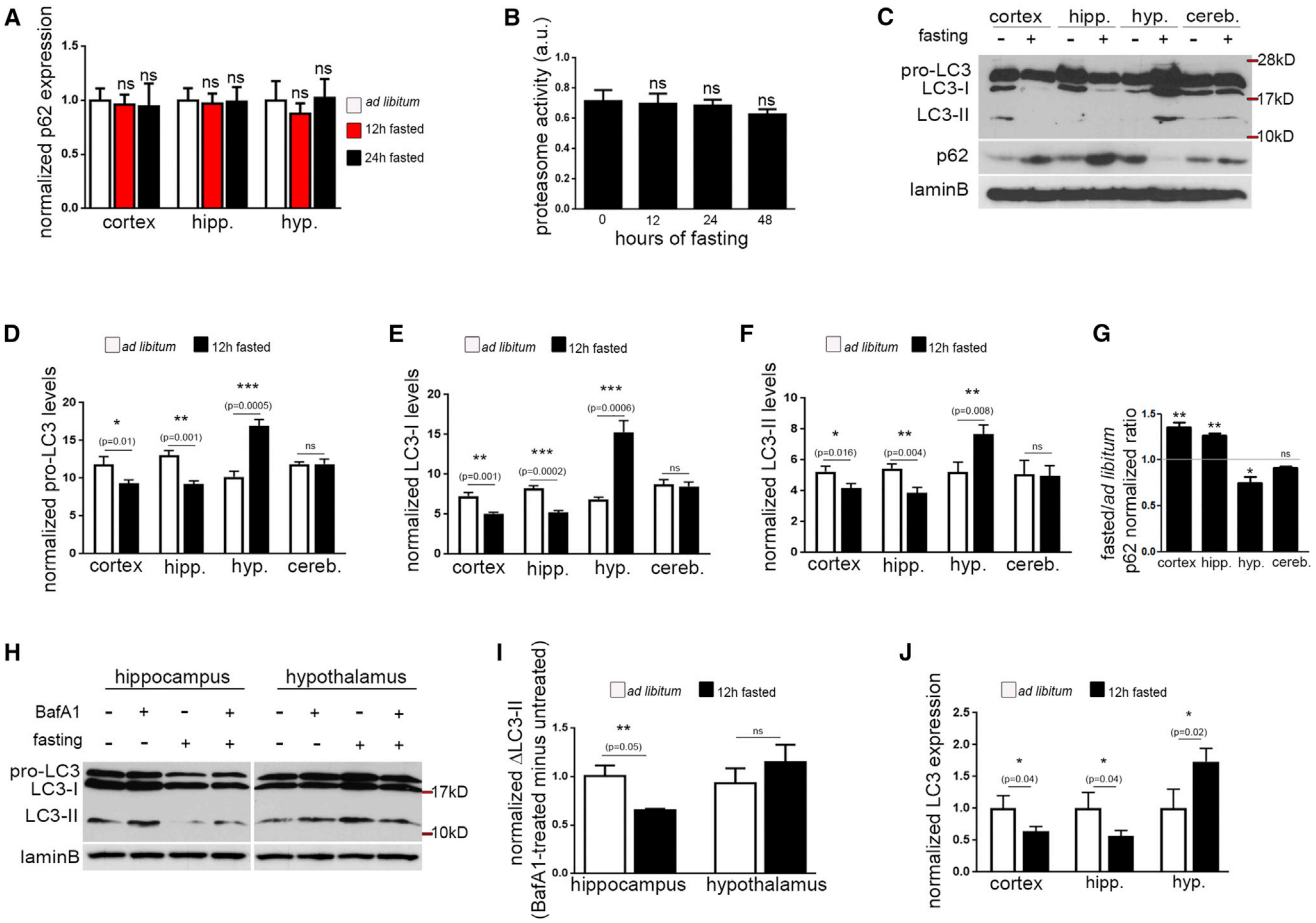

Figure 1. Differential Regulation of Autophagy across Brain Regions

(A) Graph showing the normalized p62 mRNA levels in the cortex, hippocampus, and hypothalamus of animals fed *ad libitum* or fasted for 12 or 24 hr. Bars represent mean values ± SEM. N = 6 male adult animals per condition. Statistical analyses were performed by Student's t test in all brain regions comparing each fasting time point with the *ad libitum* control.

(B) Graph showing the proteasome activity of the brain of animals fed *ad libitum* or fasted for 12, 24, or 48 hr. Bars represent mean values ± SEM. N = 6 male adult animals per condition. Statistical analyses were performed by t test comparing each fasting time point with the *ad libitum* control. All comparisons were non-significant.

(C) Protein lysates of cortex, hippocampus, hypothalamus, and cerebellum of adult male animals fed *ad libitum* or fasted for 12 hr were analyzed by western blot with antibodies against LC3 and p62, and normalized to laminB. The LC3 antibody recognizes three bands: an upper band of approximately 23 kD corresponding to pro-LC3, a middle band of 18 kD corresponding to LC3-I, and a fainter lower band of 14 kD corresponding to the lipidated LC3-II, the species that is incorporated in autophagosomes. Note that while in the hypothalamus all LC3 bands are increased upon fasting, in the cortex and hippocampus fasting causes a decrease in all LC3 bands. In the cerebellum, fasting has no effect on the levels of LC3.

(D) Graph showing the normalized levels of pro-LC3 in the cortex, hippocampus, hypothalamus, and cerebellum of mice fed *ad libitum* or fasted for 12 hr (N = 6 adult male animals fed *ad libitum* and 6 fasted for 12 hr). Bars represent mean values ± SEM. Statistical analyses were performed using Student's t test to compare *ad libitum* and fasted levels in every brain region.

(E) Graph showing the normalized levels of LC3-I in the cortex, hippocampus, hypothalamus, and cerebellum of mice fed *ad libitum* or fasted for 12 hr (N = 6 adult male animals fed *ad libitum* and 6 fasted for 12 hr). Bars represent mean values ± SEM. Statistical analyses were performed using Student's t test to compare *ad libitum* and fasted levels in every brain region.

(F) Graph showing the normalized levels of LC3-II in the cortex, hippocampus, hypothalamus, and cerebellum of mice fed *ad libitum* or fasted for 12 hr (N = 6 adult male mice fed *ad libitum* and 6 fasted for 12 hr). Bars represent mean values ± SEM. Statistical analyses were performed using Student's t test to compare *ad libitum* and fasted levels in every brain region. Note that as LC3-II levels are very low in brain lysates, we used overexposed membranes to accurately calculate its levels.

(G) Graph showing the densitometric quantification of normalized fasted to *ad libitum* ratio of p62 levels for the different brain regions. Note that this ratio is increased in the cortex and hippocampus, but decreased in the hypothalamus (N = 6 adult male mice fed *ad libitum* and 6 fasted for 12 hr). Bars represent mean values ± SEM. Statistical analyses were performed using Student's t test.

(H) Western blot analysis with an antibody against LC3 and LaminB in lysates obtained from hippocampal and hypothalamic explants. Explants were isolated from *ad libitum* or 12 hr fasted animals and cultured for 3 hr *ex vivo* in cerebrospinal fluid alone or in the presence of BafA1.

(I) Graph showing the normalized difference in LC3-II levels between BafA1-treated and untreated explants per region (hippocampus or hypothalamus) and per condition (*ad libitum* or fasted). Note that fasting causes a marked decrease in the hippocampal autophagic flux (N = 3 adult male mice per condition). Bars represent mean values ± SEM. Statistical analyses were performed using Student's t test.

(legend continued on next page)

GFP-LC3 transgene (Alirezaei et al., 2010; Klionsky et al., 2016), we sought to determine autophagic activity by monitoring levels of two endogenous proteins, LC3 and p62 (also known as SQSTM1), using naive, wild-type mice.

LC3 is produced as a pro-protein, pro-LC3, which is cleaved by ATG4B to generate the cytosolic LC3-I species. LC3-I can then be conjugated to the highly lipophilic phosphatidylethanolamine (PE) moiety to generate LC3-II, a species that integrates into lipid membranes of phagophores and autophagosomes (Barth et al., 2010) and is the only reliable marker that associates with these structures (Klionsky et al., 2016). Therefore, induction or suppression of autophagy is determined by monitoring the conversion of LC3-I to LC3-II. To ensure that this conversion reflects changes in autophagic activity, selective inhibitors of autophagosome-lysosome fusion that lead to LC3-II accumulation are used to calculate the autophagic flux (Klionsky, 2016; Klionsky et al., 2016). However, such inhibitors don't cross the blood-brain barrier and therefore cannot be applied to monitoring the autophagic flux in the brain *in vivo*.

To circumvent these limitations, concomitantly to LC3, we also monitored the levels of endogenous p62, an autophagic adaptor and substrate known to accumulate in cells when the autophagic activity is decreased (Komatsu et al., 2007). To ensure that changes in p62 levels, along with changes in LC3, can reliably monitor the autophagic activity in the brain, we first excluded the possibility that fasting affects the transcription of p62, or the activity of the proteasome, which could potentially affect p62 levels independently of autophagy. We found that p62 mRNA levels in the brain are not altered after 12 or 24 hr of fasting (Figure 1A) and that similarly, the proteasome activity is also unaffected after 12, 24, and 48 hr of fasting (Figure 1B).

Brains of adult male mice that were fed *ad libitum* or fasted for 12 hr were micro-dissected to isolate separately the cortex, hippocampus, hypothalamus, and cerebellum and determine the regulation of autophagy in each region. We found that different brain regions regulate autophagy differentially in response to fasting. In the hypothalamus, we observed that all species of LC3 (pro-LC3, LC-I, and LC3-II) are upregulated by fasting, while p62 levels are decreased (Figures 1C–1G). Taken together, these results suggest that autophagic activity is induced in the hypothalamus by fasting, as previously shown (Kaushik et al., 2011). By contrast, in the cortex and the hippocampus fasting caused a marked decrease in all LC3 species (Figures 1C–1F) and a concomitant increase in p62 levels (Figures 1C and 1G), suggesting that autophagic activity is suppressed. Finally, in the cerebellum we didn't detect changes in the levels of any LC3 species or in p62, suggesting that autophagic activity is unaffected.

To gain further confidence, we performed *ex vivo* experiments with hippocampal and hypothalamic explants, isolated from adult male animals that were fed *ad libitum* or fasted for 12 hr. Explants were maintained for 3 hr *ex vivo* in oxygenated cerebrospinal fluid in the presence or absence of bafilomycin A1 (BafA1), a selective inhibitor of the fusion between autophagosomes and lysosomes. Protein lysates were isolated from the explants and the levels of LC3 species were assessed by western blot analysis. As expected, BafA1 caused a significant accumulation of LC3-II in the hippocampus of control animals that were fed *ad libitum*. By contrast, however, fasting caused a marked decrease in the levels of all LC3 species, and BafA1 treatment resulted only in a small augmentation of the LC3-II signal in the fasted hippocampus (Figure 1H). The difference in the amount of LC3-II between BafA1-treated and untreated animals has been quantified per condition (Figure 1I), and it reflects the amount of LC3 that is delivered to the lysosome for degradation. These results indicate that fasting causes a reduction in the autophagic flux in the hippocampus. In hypothalamic explants of control mice that were fed *ad libitum*, BafA1 treatment also caused a significant accumulation of LC3-II. Fasting resulted in increased levels of all LC3 species in the hypothalamus; however, BafA1 treatment did not result in a marked further accumulation of the LC3-II signal (Figures 1H and 1I).

The fact that in the hypothalamus, cortex, and hippocampus the levels of all LC3 species are affected by fasting raises the possibility that in these brain regions, fasting regulates LC3 at the transcriptional level. Suppression or induction of autophagy by transcriptional regulation of LC3 has been previously described in several tissues (Cao et al., 2011; Kang et al., 2012; Moresi et al., 2012; Seo et al., 2011), including neurons (Xu et al., 2011), as reviewed in Füllgrabe et al. (2014). Therefore, we measured the expression of LC3 and found that fasting causes a depletion of LC3 transcripts in the cortex and hippocampus, but an upregulation in the hypothalamus (Figure 1J), indicating that the effects are indeed transcriptional.

Intrigued by the unconventional suppression of autophagy by fasting in the forebrain region, we set out to determine whether this is an inherent feature of the forebrain or a characteristic acquired with maturation. To this end, we analyzed three different postnatal ages, postnatal day 30 (P30), P70, and P90 (Figure S1). We found that at P30, fasting elicits an increase in LC3 protein and mRNA levels (Figure S1), suggestive of a classical autophagy induction. However, at P70 we start observing the reversal of this pattern, which is fully consolidated at P90 with decreased LC3 levels upon fasting (Figures S1A–S1D). We also tested the response of the hypothalamus at the same ages and found that unlike the forebrain, it responds to fasting with increased LC3 protein and mRNA levels at all ages (Figure S1). Moreover, we observed across different brain regions that the steady-state levels of LC3 at baseline were lower at P30 compared to older ages.

Regulation of Autophagy in the Brain Is Paralleled by Changes in BDNF Levels

Previous work has established that fasting results in a vast depletion of hypothalamic BDNF transcripts, driven by decreased glucose levels (Unger et al., 2007). By contrast, dietary restriction has been shown to enhance BDNF expression in the hippocampus (Lee et al., 2002). In line with this, we found increased BDNF mRNA levels in the forebrain of mice that fasted

(J) Graph showing normalized LC3 mRNA levels in the cortex, hippocampus, and hypothalamus of mice fed *ad libitum* or fasted for 12 hr (N = 6 adult male mice fed *ad libitum* and 6 fasted for 12 hr). Bars represent mean values ± SEM. Statistical analyses were performed using Student's t test to compare *ad libitum* and fasted levels in every brain region. Note that fasting causes a significant decrease in LC3 expression in the cortex and hippocampus, but an increase in the hypothalamus.

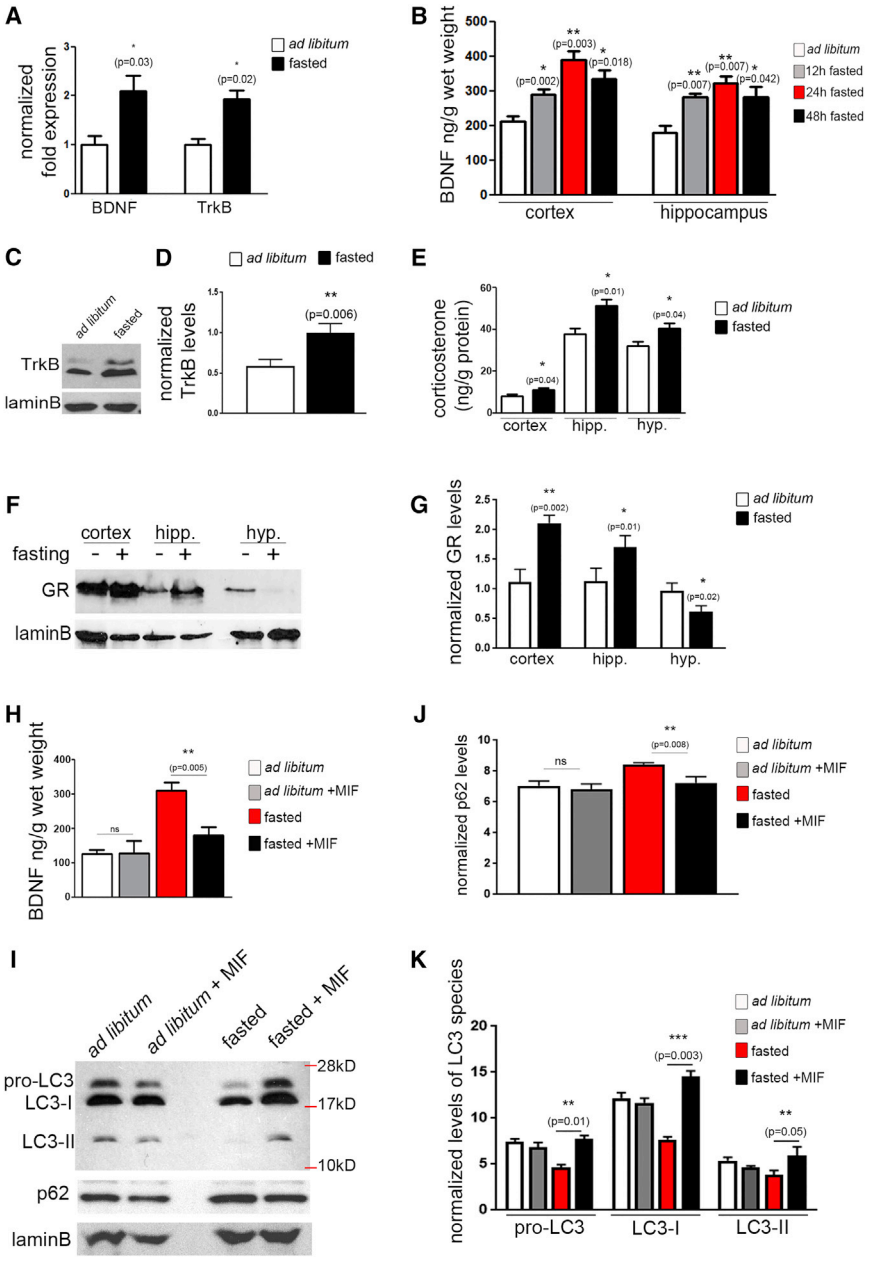

Figure 2. Regulation of Autophagy Is Paralleled by Changes in BDNF

(A) Graph showing normalized expression of BDNF and TrkB in the forebrain of adult male mice that were either fed *ad libitum* or fasted for 24 hr (N = 6 male adult mice per condition).

(B) Graph showing BDNF protein levels as determined by an ELISA assay in the cortex and hippocampus of mice fed *ad libitum* or fasted for the indicated periods of time (N = 3 adult male mice per condition). Bars represent mean values ± SEM. Statistical analyses were performed using Student's t test to compare the values of each fasted time point with the corresponding *ad libitum* control.

(C) Western blot analysis with an antibody against TrkB in forebrain lysates of mice fed *ad libitum* or fasted for 24 hr. LaminB was used as a loading control.

(D) Graph showing quantification of TrkB levels in the forebrain of mice fed *ad libitum* or fasted for 24 hr (N = 3 adult male animals fed *ad libitum* and 3 fasted). Bars represent mean values ± SEM. Statistical analysis was performed using Student's t test.

(E) Graph showing corticosterone protein levels as determined by an ELISA assay in the cortex, hippocampus, and hypothalamus of mice fed *ad libitum* or fasted for 24 hr (N = 3 adult male animals per condition). Bars represent mean values ± SEM. Statistical analysis was performed using Student's t test.

(F) Western blot analysis for the glucocorticoid receptor (GR), normalized to laminB, in lysates of cortex, hippocampus, and hypothalamus of mice fed ad libitum or fasted for 24 hr. Note that fasting increases GR levels in the cortex and hippocampus but decreases them in the hypothalamus (N = 3 adult male animals per condition). Bars represent mean values ± SEM. Statistical analysis was performed using Student's t test.

(G) Graph showing densitometric quantification of GR levels (N = 3 adult male animals per condition). Bars represent mean values ± SEM. Statistical analysis was performed using Student's t test.

(H) BDNF protein levels as determined by ELISA assay in the hippocampus of mice fed *ad libitum* or fasted for 24 hr, in the presence or absence of mifepristone (MIF) (N = 6 adult male animals per condition). Note that MIF abrogates the fasting-induced increase of BDNF levels. Bars represent mean values ± SEM. Statistical analysis was performed using Student's t test.

(I) Western blot with antibodies against LC3 and p62, and normalized to laminB in forebrain lysates of animals after 24 hr of injection with vehicle or mifepristone (MIF). Additionally, animals were fed *ad libitum* or fasted for 24 hr (starting immediately after the vehicle or MIF injection).

(J) Graph showing normalized levels of LC3 species (pro-LC3, LC3-I, and LC3-II) in the indicated conditions. Note that MIF abrogates the fasting-induced decrease of LC3 protein levels (N = 6 adult male animals per condition). Error bars represent mean values ± SEM. Statistical analyses were performed by t test.

(K) Graph showing normalized levels of p62 in the indicated conditions. Note that MIF abrogates the fasting-induced increase of p62 protein levels (N = 6 adult male animals per condition). Error bars represent mean values ± SEM. Statistical analyses were performed using Student's t test.

for 24 hr compared to *ad libitum* controls. To verify this at the protein level, we performed ELISA assay in the cortex and hippocampus of mice fed *ad libitum* or fasted for 12, 24, or 48 hr. Consistent with the expression data, we found that BDNF protein levels are increased as early as 12 hr after fasting both in the cortex and the hippocampus (Figures 2A and 2B). Therefore, while fasting causes a decrease in BDNF levels and induction of autophagy in the hypothalamus, in sharp contrast, it causes an increase in BDNF levels and suppression of autophagy in the forebrain. We also assessed the expression of TrkB, the cognate receptor of BDNF, and found that after 24 hr of fasting, TrkB mRNA and protein levels are significantly increased (Figures 2A, 2C, and 2D).

Notably, fasting had no effect on the expression of NT3, a neurotrophin that is highly related to BDNF and is also expressed in the forebrain, or its receptor TrkC (Figure S2A).

Several metabolites are known to modulate the expression of BDNF, most notable of which are steroid hormones, such as corticosterone and progesterone (Pluchino et al., 2013; Revest et al., 2014). While progesterone protein levels are not affected by fasting (Figure S2B), levels of corticosterone are increased in all brain regions tested (Figure 2G), as determined by ELISA assay. We next tested the levels of the glucocorticoid receptor (GR) and found that they are increased in the cortex and the hippocampus, but they are dramatically decreased in the hypothalamus upon fasting (Figures 2F and 2G).

Taken together, these results demonstrate that fasting regulates BDNF expression in a diametrically opposite manner between the forebrain and the hypothalamus, which is at least partly mediated by glucocorticoid signaling. To test whether the fasting-induced increase in BDNF levels in the cortex and hippocampus is mediated by corticosterone, mice were administered mifepristone, a selective inhibitor of progesterone and glucocorticoid receptors. We found that treatment with mifepristone for 24 hr prevents the fasting-induced increase of BDNF in the forebrain (Figure 2H). Notably, mifepristone treatment also prevents the suppression of LC3 levels and increase of p62 levels in the forebrain upon fasting (Figures 2I–2K), although it has no effect on p62 mRNA levels (Figure S3). These findings invite the speculation of a direct link between BDNF levels and autophagic activity.

BDNF Signaling Suppresses the Autophagic Flux in Neurons

To test the hypothesis that BDNF may directly regulate autophagy, we first treated *in vitro* cultures of hippocampal neurons with 50 or 100 ng/mL recombinant BDNF and assessed the effect on LC3 and p62 after 24 hr. We found that BDNF treatment causes a marked decrease in the levels of all LC3 forms and an increase in the levels of p62 in a dose-dependent manner (Figures 3A–3E). Treatment with K252a, a specific inhibitor of TrkB transactivation, largely abrogates the effect, indicating that BDNF acts via its cognate receptor TrkB to modulate these autophagic proteins (Figures 3A–3E). In line with these findings, immunocytochemical analysis of BDNF-treated hippocampal neurons with an antibody against LC3 revealed fewer LC3-positive autophagosomes that appear as puncta compared to untreated controls. This effect is largely abrogated in the presence of K252a (Figure 3F).

Ligation of TrkB by BDNF leads to the activation of three distinct signaling pathways, the MAP/ERK pathway, the PI3K/Akt pathway, and the PLCγ pathway (Figure S4A). To delineate the pathway involved in the suppression of autophagy, we used the following selective inhibitors for each pathway, which have been previously widely used: PD98059 and U0126 to inhibit the MAP/ERK pathway, LY294002 to inhibit the PI3K/Akt pathway, and xestospongin A to inhibit the PLCγ pathway (Figure S4A). We first assessed the effect of each inhibitor alone on the autophagic flux by calculating the ratio of LC3-II/LC3-I protein levels in the presence over absence of BafA1 (Figure S4B). We found that none of these inhibitors have any effect on the autophagic flux of hippocampal neurons after 24 hr of treatment.

To determine the pathway responsible for the effects of BDNF on LC3 and p62 protein levels, we treated neurons with BDNF in the presence of each inhibitor for 24 hr. We found that while ERK and PLCγ inhibitors do not abrogate the BDNF-induced suppression of autophagy, the PI3K inhibitor largely abolishes the effects of BDNF on LC3 and p62 levels (Figures 3A–3E). As mTOR signaling is activated by the PI3K/Akt pathway and is a major inhibitor of autophagy, we also tested the effect of rapamycin, a selective inhibitor of mTORC1. We found that rapamycin treatment abrogates the effect of BDNF on LC3 and p62 levels (Figures 3A–3E), while treatment with rapamycin alone causes a mild enhancement of baseline autophagic flux in control neurons (Figure S4B).

To determine whether BDNF suppresses the autophagic flux in neurons, we performed an LC3 assay in the presence of BafA1 to further verify that BDNF suppresses autophagic flux via the PI3K pathway. BafA1 caused an accumulation of LC3-II in untreated (control) neurons and in neurons treated with BDNF and LY294002, but not in neurons treated with BDNF alone (Figures 3F and 3G). These observations confirm that BDNF triggers depletion of autophagosomes and reduced autophagic flux, an effect that is abrogated by inhibition of the PI3K pathway.

In addition, control or BDNF-treated neurons, cultured either in the presence or absence of BafA1, were immunostained with an antibody against LC3.While BafA1 treatment caused an increase in LC3-positive puncta in control neurons (Figure 3I), it failed to do so in BDNF-treated neurons, further demonstrating that BDNF treatment suppresses the autophagic flux.

In order to determine whether BDNF suppresses the expression of specific components of the autophagic machinery, we performed qPCR analysis for transcripts of core autophagy genes in neurons treated with BDNF or not and in the forebrain of animals fed *ad libitum* or fasted (Figures 3J and 3K). We found that BDNF treatment and fasting caused the transcriptional suppression of the same set of genes, namely Atg12, LC3, and Gabarapl1, involved in elongation of the phagophore membrane and cargo recognition (Glick et al., 2010), while the expression of autophagy genes involved in induction and nucleation of the phagophore was not affected (Figures 3J and 3K).

BDNF Suppresses Autophagic Activity in the Brain

We next tested whether BDNF suppresses autophagy *in vivo* in the adult brain by analyzing animals with conditional deletion of *BDNF* in the neural lineage (*cBDNF*), obtained by crossing *Nestin-Cre* with $BDNF^{flox/flox}$ animals. In line with the *in vitro* findings, *cBDNF* mutant animals exhibit increased LC3 and decreased p62 levels (Figures 4A–4E). It is noteworthy that while all LC3 species are increased in the *cBDNF* mutant compared to control littermates, the increase in the autophagosome-associated LC3-II species is very pronounced. In addition, to exclude the possibility that changes in p62 levels may be due to transcriptional effects, we compared p62 mRNA levels in control and *cBDNF* mutant forebrains but found no significant difference (Figure S5).

To confirm that autophagy is induced in the *cBDNF* mutants, we also performed electron microscopy and counted the number

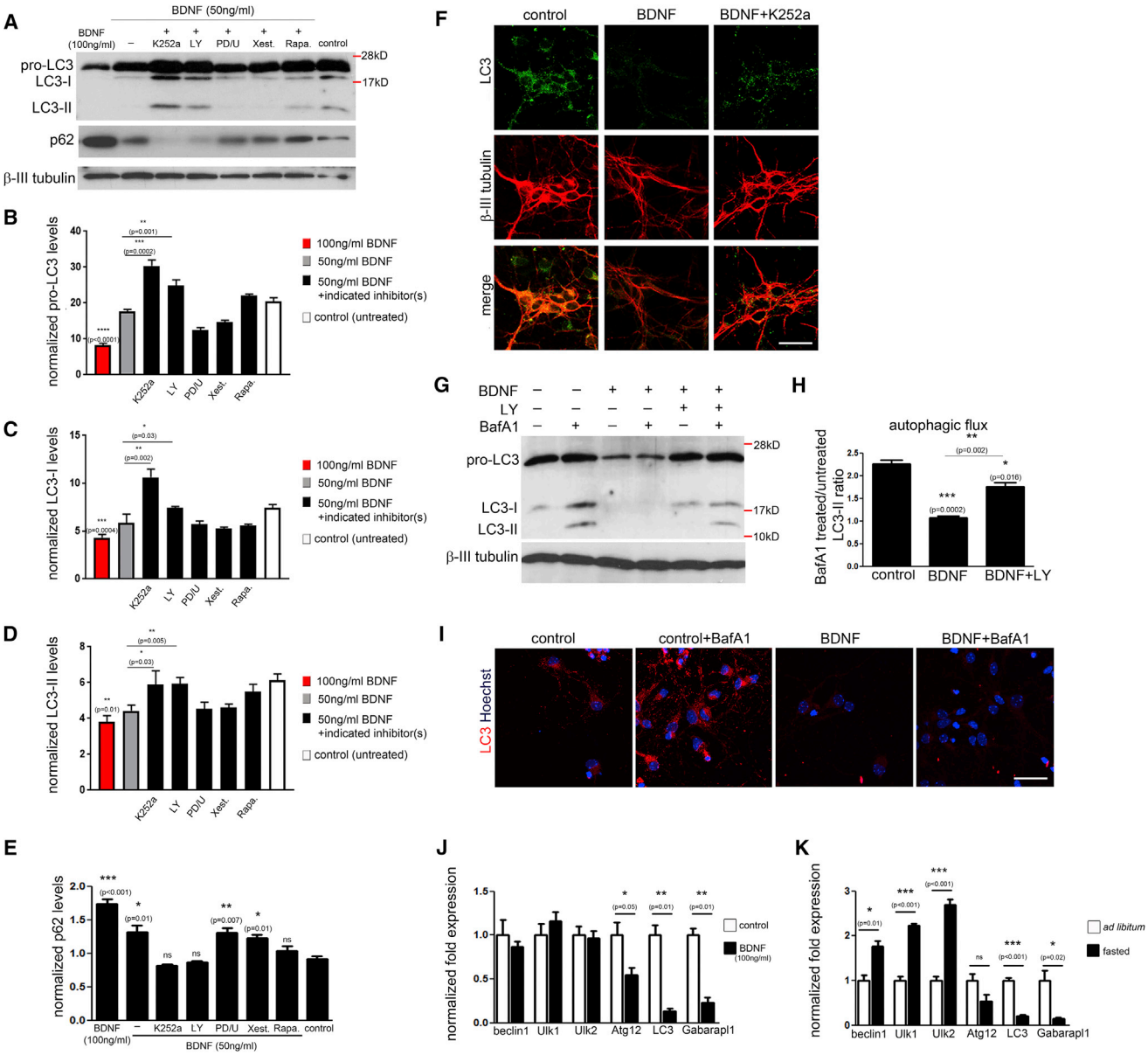

Figure 3. BDNF Directly Suppresses the Autophagic Flux in Neurons

(A) Western blot analysis with antibodies against LC3 and p62, and normalized for β-III tubulin in lysates of 21 days *in vitro* (DIV) hippocampal neurons after 24 hr of the indicated treatments. Neurons were either untreated (control) or treated with recombinant BDNF (100 or 50 ng/mL) in the presence or absence of the tyrosine kinase inhibitor K252a (0.5 μM), the MEK inhibitors (10 μM U0126 + 5 μM PD98059), the PI3K inhibitor LY294002 (LY, 50 μM), and the mTORC1 inhibitor rapamycin (10 nM).

(B) Graph showing quantification of normalized pro-LC3 levels under the indicated treatments (N = 6 independent cultures/treatment). Bars represent mean values ± SEM. Statistical analyses were performed using Student's t test. p values on single bars refer to their comparison with the untreated control.

(C) Graph showing quantification of normalized LC3-I levels under the indicated treatments (N = 6 independent cultures/treatment). Bars represent mean values ± SEM. Statistical analyses were performed using Student's t test. p values on single bars refer to their comparison with the untreated control.

(D) Graph showing quantification of normalized LC3-II levels under the indicated treatments (N = 6 independent cultures/treatment). Bars represent mean values ± SEM. Statistical analyses were performed using Student's t test. p values on single bars refer to their comparison with the untreated control.

(E) Graph showing quantification of normalized p62 levels under the indicated treatments (N = 6 independent cultures/treatment). Bars represent mean values ± SEM. Statistical analyses were performed using Student's t test. p values on single bars refer to their comparison with the untreated control.

(F) Confocal images of 21 DIV hippocampal neurons, immunostained with antibodies against LC3 and β-III tubulin. Neurons were either untreated (control), or treated for 24 hr with 100 ng/mL BDNF or with 100 ng/mL BDNF and 0.5 μM K252a. Note that BDNF reduces the number of autophagosomes (green puncta), which is largely rescued by addition of the tyrosine kinase inhibitor K252a. Scale bar, 50 μm.

(G) Western blot analysis of 21 DIV hippocampal neurons with an antibody against LC3, and normalized for β-III tubulin. Neurons were either untreated (control) or treated with the indicated combinations of 100 ng/mL BDNF, 50 μM LY294002 (LY), and 1.5 nM BafA1. BDNF and LY treatments were applied for 24 hr, while

(legend continued on next page)

of autophagosomes and autolysosomes in the CA1 region of the hippocampus. To ensure that the double-membraned structures we visualize are indeed autophagosomes, we only counted structures that we traced in at least five to ten consecutive sections. Our results revealed an overabundance of autophagosomes in the CA1 region of the *cBDNF* hippocampus compared to $BDNF^{flox/flox}$ control animals (Figures 4F and 4G). Increased numbers of autophagosomes were especially evident in presynaptic buttons and myelinated axons, where we observed more than 3-fold increase in the *cBDNF* mutant compared to $BDNF^{flox/flox}$ control, while dendrites and somas exhibited smaller increases (Figures 4F and 4G). In addition, we also observed an overabundance of lysosomes and autolysosomes in the *cBDNF* hippocampus (Figures 4H and 4I), which were mainly detected in the stratum pyramidale and localized in the somata of pyramidal neurons (Figure 4H). Therefore, we quantified the number of autolysosomes per pyramidal cell, counting only structures that could be traced in several consecutive sections, and observed a significant increase in the number of these structures (Figure 4I).

Suppression of Autophagy Is Required for BDNF-Induced Synaptic Plasticity

BDNF is an important regulator of hippocampal long-term potentiation (LTP) (Korte et al., 1995; Revest et al., 2014), a sustained enhancement of excitatory synaptic strength that underlies the processes of learning and memory. A battery of evidence indicates that BDNF acts by promoting functional and structural changes at synapses required for LTP in the hippocampus (Chen et al., 1999; Patterson et al., 1996), including in particular structural changes relevant to the number and volume of dendritic spines (Hariri et al., 2003). As autophagy has already been implicated in synaptic remodeling in various organisms (Hernandez et al., 2012; Rowland et al., 2006; Shen and Ganetzky, 2009; Tang et al., 2014), our findings raise the possibility that suppression of autophagy by BDNF may be required for synaptic plasticity.

To directly test this hypothesis, we performed LTP experiments in hippocampal slices of wild-type animals in the presence or absence of a function blocking BDNF antibody (mAb#9) (Chen et al., 1999) and the selective autophagy inhibitor (SBI-0206965) (Egan et al., 2015). We confirmed that field excitatory postsynaptic potential (fEPSP) responses are potentiated in control brain slices following theta-burst stimulation, while this potentiation is abolished when slices are pre-incubated for 6 hr with the BDNF antibody that sequesters secreted BDNF from the culture media, as previously reported (Chen et al., 1999). We then sought to determine whether suppression of autophagy can rescue the LTP defects caused by BDNF deficiency. Notably, the fEPSP was fully potentiated when brain slices were incubated in both the BDNF antibody and the autophagy inhibitor (Figures 5A–5C), demonstrating that synaptic defects of BDNF deficiency are mediated by increased autophagy. Treatment with the autophagy inhibitor alone showed a small, but not significant, enhancement of fEPSP (Figures 5A–5C). Therefore, inhibition of autophagy is sufficient to rescue the synaptic defects inflicted by loss of BDNF and restore LTP in a BDNF-deficient hippocampus paradigm.

Previous studies have indicated that fasting facilitates long-term memory in *Drosophila* (Hirano et al., 2013).Given the increased BDNF levels and suppressed autophagy in the hippocampus upon fasting, we also tested whether fasting affects memory. Notably, we found that fasted animals exhibit significantly enhanced freezing in a contextual fear conditioning test, indicating that they have increased memory compared to controls that are fed *ad libitum* (Figure 5D). Moreover, fasted animals have significantly more dendritic spines both in CA1 and CA3 regions of the hippocampus compared to controls, as revealed by Golgi-Cox staining (Figures 5E and 5F), and increased levels of PSD-95 (Figure 5G). Administration of mifepristone largely abrogates the memory enhancement of fasting, while it has little effect in control animals that are fed *ad libitum* (Figure 5H). Consistently, mifepristone also prevents the fasting-induced increase in PSD-95 protein levels (Figure 5I). Therefore, memory enhancement induced by fasting represents a physiological paradigm of synaptic adaptation mediated by increased BDNF levels and the ensuing suppression of autophagy in the adult hippocampus that increases fitness under nutritional stress.

Autophagy May Modulate Synapses by Directly Degrading Synaptic Proteins

To test the hypothesis that autophagy contributes to synaptic plasticity by degrading a specific synaptic cargo, we sought to identify indicative synaptic proteins whose degradation may be mediated by autophagy. Recognition of autophagic cargo is mainly mediated by LC3 and other Atg8-like proteins present on autophagosomal membranes that are able to interact with LC3-interacting region (LIR) motifs present on cargo. The LIR motif is generally characterized by sequences resembling W/Y/FxxI/L/V, preceded by one or two charged amino acids and where "x" represents any amino acid (Chouthai et al., 2003). Assisted by the "iLIR" server for *in silico* identification of functional

BafA1 was applied for 4 hr. Note that BafA1 causes an increase in LC3-II in control neurons and neurons treated with BDNF and LY, but not in neurons treated with BDNF alone. Also note that samples were separated on a 16% Tricine gel.

(H) Graph showing quantification of the autophagic flux in neurons. Neurons were either untreated (control) or treated with the indicated combinations of 100 ng/mL BDNF, 50 μM LY294002 (LY), and 1.5 nM BafA1. Bars represent mean values ± SEM (N = 6 independent cultures/condition). Statistical analyses were performed using Student's t test.

(I) Confocal images of 21 DIV hippocampal neurons stained with an antibody against LC3, and for the nuclear dye Hoechst. Neurons were either untreated (control), or treated with1.5 nM BafA1, 100 ng/mL BDNF, or a combination of 1.5 nM BafA1 and100 ng/mL BDNF. BDNF treatments were applied for 24 hr while BaFA1 was applied for 4 hr prior to fixation. Note that BafA1 causes an increase in LC3-II in control neurons, but not in neurons treated with BDNF. Scale bar, 50 μm.

(J) Graph showing the normalized mRNA levels of the indicated autophagy genes in hippocampal neurons that were untreated (control) or treated with 100 ng/mL BDNF. Bars represent mean values ± SEM (N = 6 independent cultures/condition). Statistical analyses were performed using Student's t test.

(K) Graph showing the normalized mRNA levels of the indicated autophagy genes in the forebrain of animals fed *ad libitum* or fasted for 24 hr (N = 3 adult male animals per condition). Bars represent mean values ± SEM. Statistical analyses were performed using Student's t test.

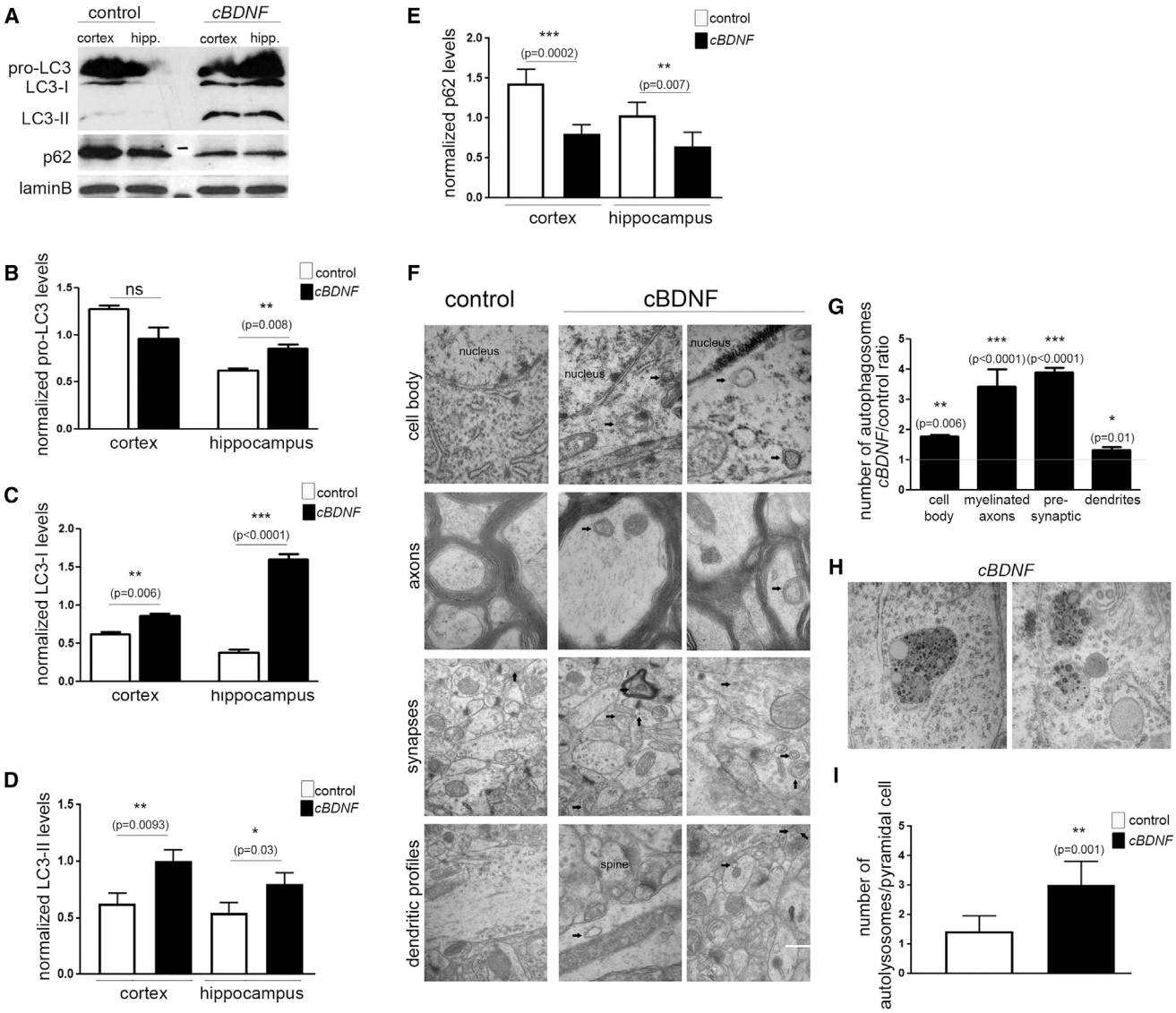

Figure 4. BDNF Suppresses Autophagic Activity in the Brain

(A) Western blot analysis of cortex and hippocampus of *BDNF*$^{f/f}$ (control) or *Nestin-Cre; BDNF*$^{f/f}$ (*cBDNF*) animals with antibodies against LC3 and p62, and normalized to laminB. Note the increased levels of LC3 species and reduced levels of p62 in the *cBDNF*.

(B) Graph showing quantification of pro-LC3 protein levels in the cortex and hippocampus of *BDNF*$^{f/f}$ (control) or *Nestin-Cre; BDNF*$^{f/f}$ (*cBDNF*) animals (N = 6 adult male animals per genotype). Bars represent mean values ± SEM. Statistical analyses were performed using Student's t test.

(C) Graph showing quantification of LC3-I protein levels in the cortex and hippocampus of *BDNF*$^{f/f}$ (control) or *Nestin-Cre; BDNF*$^{f/f}$ (*cBDNF*) animals (N = 6 adult male animals per genotype). Bars represent mean values ± SEM. Statistical analyses were performed using Student's t test.

(D) Graph showing quantification of LC3-II protein levels in the cortex and hippocampus of *BDNF*$^{f/f}$ (control) or *Nestin-Cre; BDNF*$^{f/f}$ (*cBDNF*) animals (N = 6 adult male animals per genotype). Bars represent mean values ± SEM. Statistical analyses were performed using Student's t test.

(E) Graph showing quantification of p62 protein levels in the cortex and hippocampus of *BDNF*$^{f/f}$ (control) or *Nestin-Cre; BDNF*$^{f/f}$ (*cBDNF*) animals (N = 6 adult male animals per genotype). Bars represent mean values ± SEM. Statistical analyses were performed using Student's t test.

(F) Representative electron microscopy images of autophagosomes (indicated by black arrows) from the CA1 region of the hippocampus of *BDNF*$^{f/f}$ (control) or *Nestin-Cre; BDNF*$^{f/f}$ (cBDNF) adult male mice.

(G) Graph showing the number of autophagosomes in different compartments of hippocampal pyramidal neurons as a ratio of *Nestin-Cre; BDNF*$^{f/f}$ (cBDNF) over *BDNF*$^{f/f}$ (control) mice (N = at least 20 per neuronal compartment, per genotype). Error bars ± SEM. Statistical analyses were performed by t test.

(H) Representative electron microscopy images of lysosomes and autolysosomes from the stratum pyramidale of the CA1 region of the hippocampus of *Nestin-Cre; BDNF*$^{f/f}$ (cBDNF) adult male mice, showing characteristic examples of lysosomes and autolysosomes found in the cell bodies of pyramidal neurons in this mutant.

(I) Graph showing the number of autolysosomes in the cell body of hippocampal pyramidal neurons of *BDNF*$^{f/f}$ (control) or *Nestin-Cre; BDNF*$^{f/f}$ (cBDNF) mice (N = 20 neurons per genotype). Error bars ± SEM. Statistical analyses were performed by t test.

Scale bars, 500 nm in top and bottom rows (cell body, dendritic profiles), 316 nm in second row (axons), and 630 nm in third row (synapses) (F), and 316 nm (H).

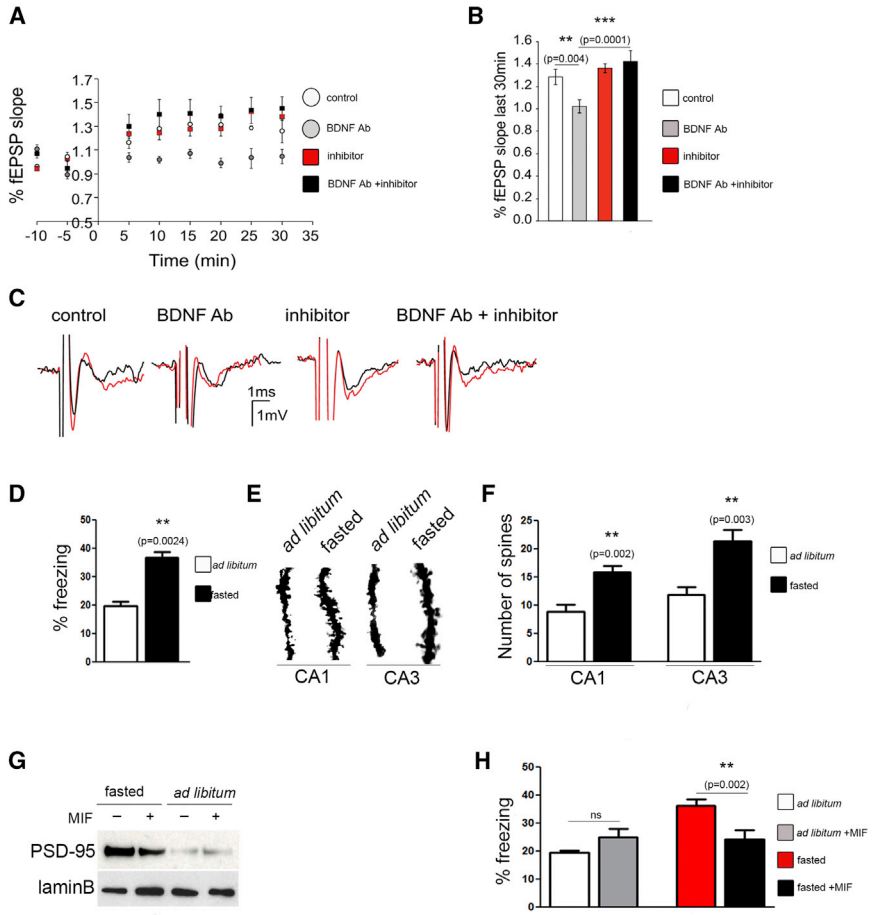

Figure 5. Suppression of Autophagy Is Required for BDNF-Induced Synaptic Plasticity

(A) Graph showing the normalized slope of fEPSP for 30 min following theta-burst stimulation of the CA3-CA1 synapses, in brain slices incubated in four different conditions: control aCSF, BDNF Ab (mAb9), autophagy inhibitor (SBI-0206965), and combination of the BDNF Ab and the autophagy inhibitor. The fEPSP responses are potentiated in the control aCSF brain slices following theta-burst stimulation, while this potentiation is abolished when the brain slices are incubated with the BDNF Ab. However, the fEPSP is potentiated when brain slices are incubated in both the BDNF Ab and the autophagy inhibitor.

(B) Graph showing the average normalized fEPSP slope 20–30 min following the theta-burst stimulation. Brain slices incubated with BDNF Ab alone showed a reduction in the potentiated fEPSP following theta-burst stimulation. This reduction was rescued when the brain slices were incubated with both the BDNF Ab and the autophagy inhibitor (N = 6 replicates per condition). Bars represent mean values ± SEM. Statistical analyses were performed using Student's t test.

(C) Representative traces of a pre-theta-burst (black) voltage response and a post-theta-burst (red) voltage response at the four different conditions.

(D) Graph showing quantification of memory as a percentage of freezing in a contextual fear conditioning paradigm in mice fed *ad libitum* or fasted (N = 6 adult male mice per condition). Bars represent mean values ± SEM. Statistical analyses were performed using Student's t test.

(E) Representative images of dendritic spines in CA1 and CA3 regions of the hippocampus as revealed by Golgi-Cox stain in hippocampal slices of adult males fed *ad libitum* or fasted.

(F) Graph showing quantification of dendritic spines in CA1 and CA3 regions of the hippocampus of mice fed *ad libitum* or fasted (N = 6 adult male mice per condition). Bars represent mean values ± SEM. Statistical analyses were performed using Student's t test.

(G) Western blot analysis for PSD-95 in hippocampal lysates of adult male mice injected with vehicle or mifepristone and fed *ad libitum* or fasted.

(H) Graph showing quantification of memory as a percentage of freezing in a contextual fear conditioning paradigm in mice injected with vehicle or mifepristone (MIF) and fed *ad libitum* or fasted (N = 6 animals per condition). Bars represent mean values ± SEM. Statistical analyses were performed using Student's t test.

LIR motifs (Egan et al., 2015), we found that three prominent scaffold proteins of dendritic spines, PSD-95, PICK1, and SHANK3, contain one or two high-fidelity LIR motifs in their sequence that are highly conserved across species (Figure 6A). To determine whether these are functional motifs, we performed immunoprecipitations of LC3 in hippocampal lysates and found that all three are co-immunoprecipitated with LC3 (Figure 6B). Consistent with being degraded by autophagy, the levels of all three proteins are significantly increased in the hippocampus of conditional *Atg5* (*cAtg5*) mutants where autophagy is ablated in the neural lineage (Figure 6C). To exclude the possibility that increased levels of these postsynaptic proteins are mediated by transcriptional upregulation in the *cAtg5* mutants, we measured their expression in the hippocampus but found no differences between control and *cAtg5* mutant animals (Figure 6D).

In order to verify that these synaptic proteins are not mere interactors of LC3 but constitute autophagic cargo, we isolated and purified autophagosomes from mouse brains. After a series of gradients, a mixed fraction of endoplasmic reticulum (ER) and autophagosomes was obtained, which, as assessed by western blot analysis, was positive for GRP78-BiP, a marker of the ER, as well as for LC3-I and LC3-II (Figure 6F). Further steps of purification separated the ER from autophagosomes, resulting in an ER fraction that was positive for GRP78-BiP but negative for LC3 and a pure autophagosomal fraction that was positive for LC3 but devoid of GRP78-BiP contamination (Figure 6F). We next performed carbonate extraction experiments on the purified autophagosomal fraction in order to break the autophagosomes, allowing us to precipitate the autophagosomal membranes as a pellet and isolate the autophagosomal content as a supernatant. As shown in Figure 6G, following this protocol, LC3-II is selectively retained in the pellet (P), while p62 is separated in the supernatant (S).

Having established this assay that allows us to biochemically isolate the content of brain autophagosomes, a fraction where the cargo is contained, we sought to investigate whether the synaptic proteins PICK1, PSD-95, and SHANK3 constitute autophagosomal cargo. To this end, we performed western blot analysis,

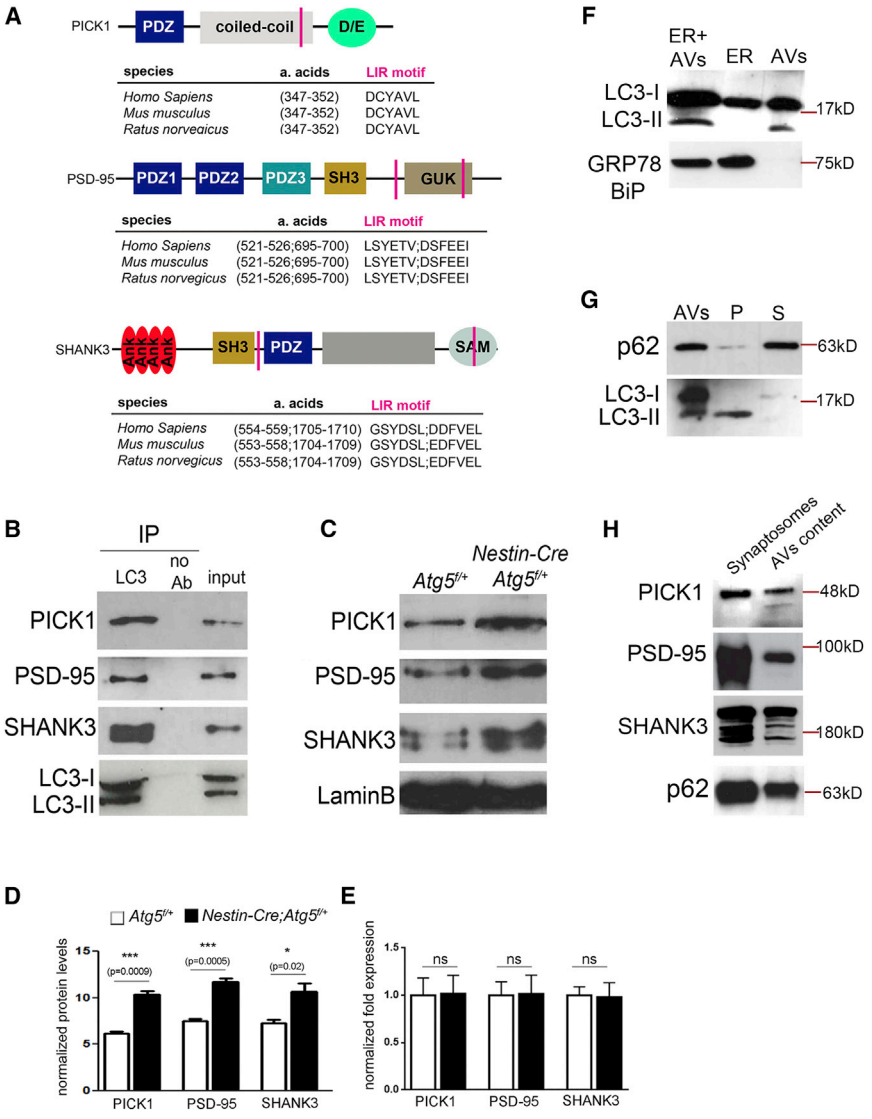

Figure 6. Autophagy May Directly Degrade Key Synaptic Proteins

(A) Schematic representation of three post-synaptic density scaffolds: PSD-95, PICK1, and SHANK3. Magenta bars indicate the location of LIR motifs. The sequences of the LIR motifs of PSD-95, PICK1, and SHANK3 are evolutionarily conserved.

(B) Immunoprecipitation with antibodies against LC3 in hippocampal lysates identifies PSD-95, PICK1, and SHANK3 as interactors of LC3.

(C) Western blot analysis with antibodies against PSD-95, PICK1, and SHANK3 in hippocampal lysates of control (*Atg5*$^{f/+}$) and conditional *Atg5* heterozygotes (*Nestin-Cre; Atg5*$^{f/+}$).

(D) Graph showing quantification of normalized PSD-95, PICK1, and SHANK3 protein levels in hippocampal lysates of control (*Atg5*$^{f/+}$) and conditional *Atg5* heterozygotes (*Nestin-Cre; Atg5*$^{f/+}$) (N = 3 adult male animals per genotype). Bars represent mean values ± SEM. Statistical analyses were performed using Student's t test.

(E) Graph showing quantification of normalized PSD-95, PICK1, and SHANK3 mRNA levels in hippocampal lysates of control (*Atg5*$^{f/+}$) and conditional *Atg5* heterozygotes (*Nestin-Cre; Atg5*$^{f/+}$) (N = 3 adult male animals per genotype). Bars represent mean values ± SEM. Statistical analyses were performed using Student's t test.

(F) Western blot analysis of different fractions along the isolation and purification of autophagosomes (AVs) from the mouse brain. The mixed fraction that contains ER and AVs is positive for both LC3 and the ER marker GRP78-BiP. However, following further purification, GRP78-BiP is retained only in the ER fraction and is missing from the purified AV fraction, while in contrast, LC3 is only retained in the AV fraction but is absent from the ER fraction.

(G) Western blot analysis with antibodies against LC3 and p62 in purified AVs and after carbonate extraction that separates the autophagosomal membranes as a pellet (P) and the autophagosomal content and a supernatant (S). Note that LC3-II is only retained in the pellet while p62 is contained in the supernatant.

(H) Western blot analysis of synaptosomes and supernatant fraction of purified brain autophagosomes with antibodies against PICK1, PSD-95, SHANK3, and p62 indicates that all three synaptic proteins are contained within autophagosomes similarly to p62.

running in parallel lysates of isolated synaptosomes, where these proteins are abundant, and the fraction of purified autophagosomal content. As shown in Figure 6H, we found that, indeed, PICK1, PSD-95, and SHANK3 are all present inside autophagosomes, similar to p62, and therefore constitute substrates of autophagy.

DISCUSSION

Our work elucidates a critical role for BDNF in regulating autophagy in the brain. Our findings demonstrate that BDNF signaling via its receptor TrkB and the PI3K pathway regulates autophagy by transcriptionally suppressing key components of the autophagic machinery required for early steps of phagophore nucleation and elongation. It is worth noting that regulation of autophagic activity by transcriptional regulation of autophagic components has been described in numerous cases, reviewed in Füllgrabe et al. (2014). For example, HDAC1 and HDAC2 were recently shown to transcriptionally regulate the autophagic flux and maintain skeletal muscle homeostasis (Moresi et al., 2012).

Previous work has implicated autophagy in the BDNF-dependent survival of hippocampal neurons upon withdrawal of serum or B27 supplement from the culture medium (Smith et al., 2014). More specifically, mTOR activation was found to be necessary for BDNF-dependent survival of rat primary hippocampal neurons under these conditions. Surprisingly, however, BDNF did not promote neuron survival by upregulating mTOR-dependent protein synthesis or through mTOR-dependent suppression of caspase-3 activation but through suppression of autophagic

flux (Smith et al., 2014). As these experiments were performed *in vitro* under conditions of supplement withdrawal that recapitulate fasting, they suggest that upregulation of neuronal autophagy is detrimental for hippocampal neurons and leads to their demise, and that BDNF mediates its pro-survival effects under these conditions by suppressing the autophagic flux. In line with this notion, our findings indicate that a glucocorticoid-signaling-mediated upregulation of BDNF in the hippocampus is activated by fasting in order to not only prevent a detrimental increase in autophagic flux, but also cause a suppression of the flux below baseline, conferring positive effects in synapse remodeling and in behavioral adaptation.

Moreover, genetic ablation of BDNF in the neural lineage results in uncontrolled increase of autophagy in the adult brain and is also associated with severe synaptic defects. Our findings demonstrate that increased autophagy is responsible for the LTP defects caused by BDNF deficiency, indicating that autophagy is a crucial component of the BDNF signaling mediating synaptic plasticity. The effects of autophagy in synapses are likely mediated by direct autophagic degradation of key synaptic protein substrates. We have indicatively identified the SHANK3, PSD-95, and PICK1 postsynaptic scaffolds, which are crucial for dendritic spine remodeling, as substrates of autophagic degradation. It is interesting that mutations in all three proteins have been implicated in autism spectrum disorders, and similarly autistic individuals were also found to have mutations that cluster in autophagy genes (Poultney et al., 2013). Deciphering the complete synaptic cargo of autophagy and understanding how its aberrant degradation contributes to neural disease are forthcoming challenges.

Our findings also reveal that autophagy, a major catabolic process, is differentially, and indeed opposingly, regulated across various regions of the adult brain upon fasting. In the forebrain, fasting causes severe suppression of the autophagic process, an unanticipated response that is at odds with that normally elicited in most other tissues, and which is mechanistically mediated by increased BDNF levels. Notably, this response is acquired with neuronal maturation and consolidated only at 3 months of age, in line with the notion that higher centers in the cortex continue to mature into the early adulthood. Such an example is the prefrontal cortex, which has a prolonged development, allowing the acquisition of complex cognitive abilities through experience.

By contrast, and in line with previous reports (Kaushik et al., 2011), the hypothalamus responds to fasting in a classical manner, namely by increasing its autophagic flux. Since these two regions are involved in distinct tasks, these differences argue that different neuronal types regulate catabolism in unique ways that serve their specific functions. In line with this notion, induction of autophagy in the hypothalamus by fasting is essential for mobilizing neuron-intrinsic lipids to generate free fatty acids and to ultimately upregulate Agouti-related peptide (AgRP), the neuropeptide that acts as a natural antagonist for the melanocortin receptors to invoke food intake (Kaushik et al., 2011). Therefore, autophagy is positively regulated in hypothalamic neurons responsible for food intake in order to confer the neuropeptide changes that mediate the adaptive response of the accompanying feeling of hunger. The possible contribution of BDNF depletion in the induction of autophagy in the hypothalamus upon fasting is thus worth considering in the future.

STAR★METHODS

Detailed methods are provided in the online version of this paper and include the following:

- KEY RESOURCES TABLE
- CONTACT FOR REAGENT AND RESOURCE SHARING
- METHOD DETAILS
  - Mouse Models
  - Fasting Protocol
  - Dissection of Different Brain Regions
  - Ex Vivo Autophagy Assay
  - Enzyme-Linked Immunosorbent Assay (ELISA) and Proteasome Activity Assay
  - Western Blotting
  - Immunoprecipitations
  - Quantitative RT-PCR
  - Contextual Fear Conditioning
  - Golgi-Cox staining
  - Electrophysiology
  - Electron Microscopy
  - Neuronal Cultures
  - Immunostaining
  - Isolation of Autophagosomes from the Brain
- QUANTIFICATION AND STATISTICAL ANALYSIS

SUPPLEMENTAL INFORMATION

Supplemental Information includes five figures and can be found with this article online at http://dx.doi.org/10.1016/j.cmet.2017.06.005.

AUTHOR CONTRIBUTIONS

V.N. and N.T. designed the study. V.N. performed experiments and analyzed data. K.S. conducted electrophysiology, E.K. performed autophagosome isolation experiments, and Y.D. performed electron microscopy analyses. V.N. and N.T. wrote the manuscript.

ACKNOWLEDGMENTS

We thank A. Pasparaki for technical support with confocal imaging, Prof. M. Sendtner for the *BDNF*$^{flox/flox}$ mice, and Prof. A. Iliopoulos for the *Atg5*$^{flox/flox}$ mice. This work was funded by a Marie-Curie career restart fellowship (628649_Mitoneuromage) to V.N. and by grants from the European Research Council (ERC 233358 - NeuronAge) and the European Commission 7th Framework Programme (Marie Curie Initial Training Network 316354 CodeAge).

Received: January 20, 2016
Revised: February 10, 2017
Accepted: June 9, 2017
Published: July 5, 2017

REFERENCES

Alirezaei, M., Kemball, C.C., Flynn, C.T., Wood, M.R., Whitton, J.L., and Kiosses, W.B. (2010). Short-term fasting induces profound neuronal autophagy. Autophagy *6*, 702–710.

Alvarez-Castelao, B., and Schuman, E.M. (2015). The regulation of synaptic protein turnover. J. Biol. Chem. *290*, 28623–28630.

Barth, S., Glick, D., and Macleod, K.F. (2010). Autophagy: assays and artifacts. J. Pathol. *221*, 117–124.

Berg, T.O., Fengsrud, M., Strømhaug, P.E., Berg, T., and Seglen, P.O. (1998). Isolation and characterization of rat liver amphisomes. Evidence for fusion of autophagosomes with both early and late endosomes. J. Biol. Chem. *273*, 21883–21892.

Cao, D.J., Wang, Z.V., Battiprolu, P.K., Jiang, N., Morales, C.R., Kong, Y., Rothermel, B.A., Gillette, T.G., and Hill, J.A. (2011). Histone deacetylase (HDAC) inhibitors attenuate cardiac hypertrophy by suppressing autophagy. Proc. Natl. Acad. Sci. USA *108*, 4123–4128.

Chen, G., Kolbeck, R., Barde, Y.A., Bonhoeffer, T., and Kossel, A. (1999). Relative contribution of endogenous neurotrophins in hippocampal long-term potentiation. J. Neurosci. *19*, 7983–7990.

Chouthai, N.S., Sampers, J., Desai, N., and Smith, G.M. (2003). Changes in neurotrophin levels in umbilical cord blood from infants with different gestational ages and clinical conditions. Pediatr. Res. *53*, 965–969.

Dalezios, Y., Luján, R., Shigemoto, R., Roberts, J.D., and Somogyi, P. (2002). Enrichment of mGluR7a in the presynaptic active zones of GABAergic and non-GABAergic terminals on interneurons in the rat somatosensory cortex. Cereb. Cortex *12*, 961–974.

Dong, X.X., Wang, Y.R., Qin, S., Liang, Z.Q., Liu, B.H., Qin, Z.H., and Wang, Y. (2012). p53 mediates autophagy activation and mitochondria dysfunction in kainic acid-induced excitotoxicity in primary striatal neurons. Neuroscience *207*, 52–64.

Egan, D.F., Chun, M.G., Vamos, M., Zou, H., Rong, J., Miller, C.J., Lou, H.J., Raveendra-Panickar, D., Yang, C.C., Sheffler, D.J., et al. (2015). Small molecule inhibition of the autophagy kinase ULK1 and identification of ULK1 substrates. Mol. Cell *59*, 285–297.

Füllgrabe, J., Klionsky, D.J., and Joseph, B. (2014). The return of the nucleus: transcriptional and epigenetic control of autophagy. Nat. Rev. Mol. Cell Biol. *15*, 65–74.

Glick, D., Barth, S., and Macleod, K.F. (2010). Autophagy: cellular and molecular mechanisms. J. Pathol. *221*, 3–12.

Hara, T., Nakamura, K., Matsui, M., Yamamoto, A., Nakahara, Y., Suzuki-Migishima, R., Yokoyama, M., Mishima, K., Saito, I., Okano, H., and Mizushima, N. (2006). Suppression of basal autophagy in neural cells causes neurodegenerative disease in mice. Nature *441*, 885–889.

Hariri, A.R., Goldberg, T.E., Mattay, V.S., Kolachana, B.S., Callicott, J.H., Egan, M.F., and Weinberger, D.R. (2003). Brain-derived neurotrophic factor val66met polymorphism affects human memory-related hippocampal activity and predicts memory performance. J. Neurosci. *23*, 6690–6694.

Hernandez, D., Torres, C.A., Setlik, W., Cebrián, C., Mosharov, E.V., Tang, G., Cheng, H.C., Kholodilov, N., Yarygina, O., Burke, R.E., et al. (2012). Regulation of presynaptic neurotransmission by macroautophagy. Neuron *74*, 277–284.

Hirano, Y., Masuda, T., Naganos, S., Matsuno, M., Ueno, K., Miyashita, T., Horiuchi, J., and Saitoe, M. (2013). Fasting launches CRTC to facilitate long-term memory formation in Drosophila. Science *339*, 443–446.

Kang, Y.A., Sanalkumar, R., O'Geen, H., Linnemann, A.K., Chang, C.J., Bouhassira, E.E., Farnham, P.J., Keles, S., and Bresnick, E.H. (2012). Autophagy driven by a master regulator of hematopoiesis. Mol. Cell. Biol. *32*, 226–239.

Kaushik, S., Rodriguez-Navarro, J.A., Arias, E., Kiffin, R., Sahu, S., Schwartz, G.J., Cuervo, A.M., and Singh, R. (2011). Autophagy in hypothalamic AgRP neurons regulates food intake and energy balance. Cell Metab. *14*, 173–183.

Klionsky, D.J. (2016). Stepping back from the guidelines: Where do we stand? Autophagy *12*, 223–224.

Klionsky, D.J., Abdelmohsen, K., Abe, A., Abedin, M.J., Abeliovich, H., Acevedo Arozena, A., Adachi, H., Adams, C.M., Adams, P.D., Adeli, K., et al. (2016). Guidelines for the use and interpretation of assays for monitoring autophagy (3rd edition). Autophagy *12*, 1–222.

Koike, M., Shibata, M., Tadakoshi, M., Gotoh, K., Komatsu, M., Waguri, S., Kawahara, N., Kuida, K., Nagata, S., Kominami, E., et al. (2008). Inhibition of autophagy prevents hippocampal pyramidal neuron death after hypoxic-ischemic injury. Am. J. Pathol. *172*, 454–469.

Kolbeck, R., Bartke, I., Eberle, W., and Barde, Y.A. (1999). Brain-derived neurotrophic factor levels in the nervous system of wild-type and neurotrophin gene mutant mice. J. Neurochem. *72*, 1930–1938.

Komatsu, M., Waguri, S., Chiba, T., Murata, S., Iwata, J., Tanida, I., Ueno, T., Koike, M., Uchiyama, Y., Kominami, E., and Tanaka, K. (2006). Loss of autophagy in the central nervous system causes neurodegeneration in mice. Nature *441*, 880–884.

Komatsu, M., Waguri, S., Koike, M., Sou, Y.S., Ueno, T., Hara, T., Mizushima, N., Iwata, J., Ezaki, J., Murata, S., et al. (2007). Homeostatic levels of p62 control cytoplasmic inclusion body formation in autophagy-deficient mice. Cell *131*, 1149–1163.

Korte, M., Carroll, P., Wolf, E., Brem, G., Thoenen, H., and Bonhoeffer, T. (1995). Hippocampal long-term potentiation is impaired in mice lacking brain-derived neurotrophic factor. Proc. Natl. Acad. Sci. USA *92*, 8856–8860.

Lee, J., Seroogy, K.B., and Mattson, M.P. (2002). Dietary restriction enhances neurotrophin expression and neurogenesis in the hippocampus of adult mice. J. Neurochem. *80*, 539–547.

Liang, C.C., Wang, C., Peng, X., Gan, B., and Guan, J.L. (2010). Neural-specific deletion of FIP200 leads to cerebellar degeneration caused by increased neuronal death and axon degeneration. J. Biol. Chem. *285*, 3499–3509.

Matsumoto, T., Rauskolb, S., Polack, M., Klose, J., Kolbeck, R., Korte, M., and Barde, Y.A. (2008). Biosynthesis and processing of endogenous BDNF: CNS neurons store and secrete BDNF, not pro-BDNF. Nat. Neurosci. *11*, 131–133.

Mizushima, N., Yamamoto, A., Matsui, M., Yoshimori, T., and Ohsumi, Y. (2004). In vivo analysis of autophagy in response to nutrient starvation using transgenic mice expressing a fluorescent autophagosome marker. Mol. Biol. Cell *15*, 1101–1111.

Moresi, V., Carrer, M., Grueter, C.E., Rifki, O.F., Shelton, J.M., Richardson, J.A., Bassel-Duby, R., and Olson, E.N. (2012). Histone deacetylases 1 and 2 regulate autophagy flux and skeletal muscle homeostasis in mice. Proc. Natl. Acad. Sci. USA *109*, 1649–1654.

Nikoletopoulou, V., Lickert, H., Frade, J.M., Rencurel, C., Giallonardo, P., Zhang, L., Bibel, M., and Barde, Y.A. (2010). Neurotrophin receptors TrkA and TrkC cause neuronal death whereas TrkB does not. Nature *467*, 59–63.

Patterson, S.L., Abel, T., Deuel, T.A., Martin, K.C., Rose, J.C., and Kandel, E.R. (1996). Recombinant BDNF rescues deficits in basal synaptic transmission and hippocampal LTP in BDNF knockout mice. Neuron *16*, 1137–1145.

Pluchino, N., Russo, M., Santoro, A.N., Litta, P., Cela, V., and Genazzani, A.R. (2013). Steroid hormones and BDNF. Neuroscience *239*, 271–279.

Poultney, C.S., Goldberg, A.P., Drapeau, E., Kou, Y., Harony-Nicolas, H., Kajiwara, Y., De Rubeis, S., Durand, S., Stevens, C., Rehnström, K., et al. (2013). Identification of small exonic CNV from whole-exome sequence data and application to autism spectrum disorder. Am. J. Hum. Genet. *93*, 607–619.

Rauskolb, S., Zagrebelsky, M., Dreznjak, A., Deogracias, R., Matsumoto, T., Wiese, S., Erne, B., Sendtner, M., Schaeren-Wiemers, N., Korte, M., and Barde, Y.A. (2010). Global deprivation of brain-derived neurotrophic factor in the CNS reveals an area-specific requirement for dendritic growth. J. Neurosci. *30*, 1739–1749.

Revest, J.M., Le Roux, A., Roullot-Lacarrière, V., Kaouane, N., Vallée, M., Kasanetz, F., Rougé-Pont, F., Tronche, F., Desmedt, A., and Piazza, P.V. (2014). BDNF-TrkB signaling through Erk1/2 MAPK phosphorylation mediates the enhancement of fear memory induced by glucocorticoids. Mol. Psychiatry *19*, 1001–1009.

Rowland, A.M., Richmond, J.E., Olsen, J.G., Hall, D.H., and Bamber, B.A. (2006). Presynaptic terminals independently regulate synaptic clustering and autophagy of GABAA receptors in Caenorhabditis elegans. J. Neurosci. *26*, 1711–1720.

Seglen, P.O., and Brinchmann, M.F. (2010). Purification of autophagosomes from rat hepatocytes. Autophagy *6*, 542–547.

Seo, Y.K., Jeon, T.I., Chong, H.K., Biesinger, J., Xie, X., and Osborne, T.F. (2011). Genome-wide localization of SREBP-2 in hepatic chromatin predicts a role in autophagy. Cell Metab. *13*, 367–375.

Shen, W., and Ganetzky, B. (2009). Autophagy promotes synapse development in Drosophila. J. Cell Biol. *187*, 71–79.

Smith, E.D., Prieto, G.A., Tong, L., Sears-Kraxberger, I., Rice, J.D., Steward, O., and Cotman, C.W. (2014). Rapamycin and interleukin-1β impair brain-derived neurotrophic factor-dependent neuron survival by modulating autophagy. J. Biol. Chem. *289*, 20615–20629.

Spijker, S. (2011). Dissection of rodent brain regions. In Neuroproteomics, K.W. Li, ed. (Springer), pp. 13–26.

Strømhaug, P.E., Berg, T.O., Fengsrud, M., and Seglen, P.O. (1998). Purification and characterization of autophagosomes from rat hepatocytes. Biochem. J. *335*, 217–224.

Tang, G., Gudsnuk, K., Kuo, S.H., Cotrina, M.L., Rosoklija, G., Sosunov, A., Sonders, M.S., Kanter, E., Castagna, C., Yamamoto, A., et al. (2014). Loss of mTOR-dependent macroautophagy causes autistic-like synaptic pruning deficits. Neuron *83*, 1131–1143.

Unger, T.J., Calderon, G.A., Bradley, L.C., Sena-Esteves, M., and Rios, M. (2007). Selective deletion of Bdnf in the ventromedial and dorsomedial hypothalamus of adult mice results in hyperphagic behavior and obesity. J. Neurosci. *27*, 14265–14274.

Xu, P., Das, M., Reilly, J., and Davis, R.J. (2011). JNK regulates FoxO-dependent autophagy in neurons. Genes Dev. *25*, 310–322.

Yue, Z., Horton, A., Bravin, M., DeJager, P.L., Selimi, F., and Heintz, N. (2002). A novel protein complex linking the delta 2 glutamate receptor and autophagy: implications for neurodegeneration in lurcher mice. Neuron *35*, 921–933.

STAR★METHODS

KEY RESOURCES TABLE

REAGENT or RESOURCE	SOURCE	IDENTIFIER
Antibodies		
Mouse monoclonal anti-MAP LC3B (G9)	Santa Cruz	sc-376404; RRID: AB_11150489
Rabbit polyclonal anti-MAP LC3B (D11) XP;	Cell Signaling	Cat# 3868; RRID: AB_2137707
Guinea pig polyclonal anti-p62 (SQSTM1)	Biogen	Cat# GP62-C
Goat polyclonal anti-Lamin B (C-20)	Santa Cruz	Cat# sc-6216; RRID: AB_648156
Mouse monoclonal anti-b-III tubulin (2G10)	Abcam	Cat# ab78078; RRID: AB_2256751
BDNF #9	DSHB	Cat# BDNF-#9; RRID: AB_2617199
Rabbit polyclonal anti-BDNF (N20)	Santa Cruz	Cat# sc-546; RRID: AB_630940
Rabbit polyclonal anti-PSD-95 (D27E11) XP	Cell Signaling	Cat# 3450; RRID: AB_2292883
Mouse monoclonal anti-Shank3 [N69/46]	Abcam	Cat# ab193307
Goat polyclonal anti-PICK-1	Abcam	Cat# ab77178; RRID: AB_2164531
Rabbit polyclonal anti-p44/42 MAPK (Erk1/2) (137F5)	Cell Signaling	Cat# 4695; RRID: AB_390779
Rabbit anti-Phospho-p44/42 MAPK (Erk1/2) (Thr202/ Tyr204) (197G2)	Cell Signaling	Cat# 4377; RRID: AB_331775
Chemicals, Peptides, and Recombinant Proteins		
K252a	Cell Signaling #12754	CAS 97161-97-2
LY294002	Cell Signaling #9901	CAS 154447-36-6
U0126	Cell Signaling #9903	CAS 109511-58-2
PD98059	Cell Signaling #9900	CAS 167869-21-8
Rapamycin	Sigma-Aldrich #553210	CAS 53123-88-9
Bafilomycin A1	Sigma-Aldrich #B1793	CAS 88899-55-2
Xestospongin A	Sigma-Aldrich	CAS 88840-02-2
SBI-0206965	Sigma-Aldrich #SML1540	PubChem ID 329825951
GPN	Cayman #14634	CAS 21438-66-4
Iodixanol	Sigma-Aldrich #Y0001294	CAS 92339-11-2
Recombinant BDNF	Alomone # B-250	N/A
Critical Commercial Assays		
Progesterone ELISA	Abcam	Cat# ab108670
Corticosterone ELISA kit	Abcam	Cat# ab108821
Proteasome Activity kit	Abcam	Cat# ab107921
Experimental Models: Organisms/Strains		
Bl6 wildtype mouse, C57BL/6J	Jax labs	Stock No:000664
BDNFflox/flox mouse	Prof. Michael Sendtner	N/A
Atg5 flox/flox mouse, B6.129S-Atg5 < tm1Myok >	RIKEN	RBRC02975
Nestin-Cre mouse, B6.Cg-Tg(Nes-cre)1Kln/J	Jax labs	Stock No:003771
Oligonucleotides		
P62; Forward primer: GCCAGAGGAACAGATGGAGT; reverse primer: TCCGATTCTGGCATCTGTAG		N/A
BDNF; Forward primer: GACAAGGCAACTTGGCCTAC; reverse primer: ATTGGGTAGTTCGGCATTGC		N/A
TrkB; Forward primer: TGAGGAGGACACAGGATGTTGA; reverse primer: TTCCAGTGCAAGCCAGTATCTG		N/A
NT3; Forward primer: GCCCCCTCCCTTATACCTAATG; reverse primer: CATAGCGTTTCCTCCGTGGT		N/A
TrkC; Forward primer: TTAGGGCAGACTCTGGGTCTCT; reverse primer: GCTTTCCAACACGGAGGTCAT		N/A

(*Continued on next page*)

Continued		
REAGENT or RESOURCE	SOURCE	IDENTIFIER
Beclin1; Forward primer: GGCCAATAAGATGGGTCTGA; reverse primer: CACTGCCTCCAGTGTCTTCA		N/A
Ulk1; Forward primer: CGTCCTCCAAGACGCTGTAT; reverse primer: CCTGTTGCTTTCCTCCAAAG		N/A
Ulk2; Forward primer: CAGCCCTGGATGAGATGTTT; reverse primer: GGATGGGTGACAGAACCAAG		N/A
LC3B; Forward primer: CGTCCTGGACAAGACCAAGT; reverse primer: ATTGCTGTCCCGAATGTCTC		N/A
Atg12; Forward primer: GGCCTCGGAACAGTTGTTTA; reverse primer: CAGCACCGAAATGTCTCTGA		N/A
Gabarapl1; Forward primer: CATCGTGGAGAAGGCTCCTA; reverse primer: ATACAGCTGGCCCATGGTAG		N/A
PICK1; Forward primer: TGAGAAGTTCGGCATTCGGC; reverse primer: GCACACACCACTCTAGCCTA		N/A
PSD-95; Forward primer: GGTGACGACCCATCCAT CTTTATC; reverse primer: CGGACATCCACTTCA TTGACAAAC		N/A
Shank3; Forward primer: ACGAAGTGCCTGCGTCTGGAC; reverse primer: CTCTTGCCAACCATTCTCATCAGTG		N/A
GAPDH; Forward primer: ACCCAGAAGACTGTGGATGG; reverse primer: CACATTGGGGGTAGGAACAC		N/A
Software and Algorithms		
GraphPad Prism		N/A

CONTACT FOR REAGENT AND RESOURCE SHARING

Further information and requests for resources and reagents should be addressed to and will be fulfilled by the Lead Contact, Nektarios Tavernarakis (tavernarakis@imbb.forth.gr).

METHOD DETAILS

Mouse Models

All animal protocols were approved by the FORTH Animal Ethics Committee (FEC). All mice were maintained in a pathogen-free environment and housed in clear shoebox cages in groups of five animals per cage with constant temperature and humidity and 12 hr/12 hr light/dark cycle. All animals used were male mice of C57BL/6 genetic background. For most experiments adult animals were used (approximately 3 months of age), while for the experiments shown in Figure S1 animals of 30, 70 and 90 days postnatal were used. *Atg5*$^{flox/flox}$ mice (a generous gift of Dr. Aris Iliopoulos) were crossed with *Nestin-Cre* mice to generate animals where *Atg5* is conditionally ablated in the neural lineage (*cAtg5*), as previously described (Hara et al., 2006). Transgenic mice in which loxP sites were inserted flanking the coding region (exon IX) of the *BDNF* gene (*BDNF*$^{flox/flox}$ mice, a generous gift of Dr. Michael Sendtner) (Cao et al., 2011) were crossed with *Nestin-Cre* mice to generate animals where BDNF is conditionally ablated in the neural lineage (*cBDNF*).

Fasting Protocol

Adult (3-4 months old) male mice of a C57BL/6 genetic background were used for fasting experiments. For fasting, mice were deprived of all food for 12, 24 or 48 hr, as indicated in different experiments, with free access to water. Control mice were given an ad libitum regime on chow (Mucedola, 4RF24 GLP).

Dissection of Different Brain Regions

Freshly isolated brains were micro-dissected on ice as previously described to separately isolate the cortex, the hippocampus, the hypothalamus and the cerebellum (Spijker, 2011). Isolated regions were immediately processed for protein or RNA extraction.

Ex Vivo Autophagy Assay

Three adult male mice were fed ad libitum and three were fasted for 12 hr. Subsequently, animals were sacrificed and their entire hippocampus and hypothalamus were isolated from each side of the brain. The hippocampus and hypothalamus from the one side were maintained in oxygenated cerebrospinal fluid alone, while the ones from the other side were supplemented with 1.5nM

BafilomycinA1 (Sigma-Aldrich). Three hours later, explants were processed for isolation of lysates, as described below under "Western blotting" and analyzed by western blot with an antibody against LC3 and loading control with an antibody against LaminB, both from Santa Cruz.

Enzyme-Linked Immunosorbent Assay (ELISA) and Proteasome Activity Assay

BDNF extraction from tissues and quantification by ELISA was performed as previously described (Kolbeck et al., 1999; Matsumoto et al., 2008; Rauskolb et al., 2010). Progesterone and corticosterone ELISA was performed using commercial kits (Abcam) and following the manufacturer's instructions. The activity of the proteasome was measured using a commercial kit (Abcam) and following the manufacturer's instructions.

Western Blotting

Western blots were performed as previously described (Nikoletopoulou et al., 2010) with slight modifications. Briefly, tissues were collected in cold PBS and lysed by sonication in RIPA buffer (500 mM Tris-HCl pH 7.2, 1 M NaCl, EDTA, Triton 100-X, Na-deoxycholate, 10% SDS), supplemented with protease inhibitors (Roche) and 1 mM dithiothreitol (DTT), and placed for 20 min on ice, followed by 20 min centrifugation at 14,000 rpm. Samples were separated on a 10% or 15% polyacrylamide gel and transferred to a nitrocellulose membrane (Millipore). After blocking for 1 hr at room temperature in 5% skim milk, membranes were incubated in the primary antibodies overnight at 4°C. The primary antibodies used were LC3 (Santa Cruz), p62 (Biogen), laminB (Santa Cruz), β-III tubulin (Santa Cruz), BDNF (mAb#9 from DSHB and N20 from Santa Cruz), PSD-95 (Cell Signaling), Shank3 (Abcam), and PICK-1(Abcam), Erk (Cell Signaling) and p-Erk (Cell Signaling). After three 5 min washes in TPBS (100 mM Na_2HPO4, 100mM NaH_2PO4, 0.5N NaCl, 0.1% Tween-20), membranes were incubated for 1 hr at room temperature in corresponding secondary horseradish peroxidase-conjugated antibodies (Abcam). Blots were developed by chemiluminescence (Supersignal chemiluminescent substrate, pico and fempto, Thermo Fisher Scientific) according to the manufacturer's instructions.

Immunoprecipitations

Immunoprecipitations were performed as previously described (Egan et al., 2015; Matsumoto et al., 2008). Briefly, lysates were pre-cleared by incubation with 30μl of protein G Agarose beads on a rotator overnight at 4°C. Pre-cleared lysates were then incubated with beads that were conjugated with an antibody against LC3 (Santa Cruz) overnight on a rotator at 4°C. The following day, beads were washed in cold lysis buffer 3 times and then used for analysis on Western Blot. No antibody and IgG controls were used in parallel to ensure specificity.

Quantitative RT-PCR

RNA isolation was performed using Trizol (Thermo Fisher Scientific), and reverse transcription was performed using iScript (Biorad), following the manufacturer's instructions respectively. qPCR was performed with KAPA SYBR FAST qPCR Kit (Kapa biosystems) following the manufacturer's instructions. For the sets of oligos used please see the Key Resources Table.

Contextual Fear Conditioning

Male mice, 2-3 months old were fed ad libitum or fasted and for some experiments they were injected once either with saline or with Mifepristone (100μl of 30mg/ml). Twenty-four hours following initiation of the fasting, mice (one at a time) were placed in the fear conditioning chamber (MedAssociates), which was controlled through a custom-made interface connected to the computer. After 7min of habituation to the conditioning chamber, each mouse received one mild electrical foot-shock (750ms, 0.75 mA), and remained in the chamber for another 5min. The next day (while ad libitum or fasting regime continued), mice were returned to the training chamber using the same context for 9 min. The freezing behavior was analyzed manually using J-Watcher software (http://www.jwatcher.ucla.edu/) from 4-7 min of the testing session.

Golgi-Cox staining

Mice were fed ad libitum (n = 5) or fasted (n = 5) for 48hrs. At that time, brains were removed and placed in Golgi-Cox solution (5% Potassium Dichromate, 5% Mercuric Chloride (sublimate), and 5% Solution of Potassium Chromate), which had been prepared at least 5 days earlier. Brains remained in Golgi-Cox solution for 10 days at room temperature, then placed in 30% sucrose solution and subsequently sliced (150 μm thick slices) in a vibratome (Leica VT1000S). The slices were placed onto gelatin-coated microscope slides, covered with parafilm, and maintained in a humidity chamber for about 30-40 hr. The parafilm was then removed, and the slides were incubated first in ammonium hydroxide for 15 min in a dark room and then in Kodak Fix solution for 15 min followed by washes with dH_2O. The brain slices were then dehydrated with increasing concentrations of ethanol, incubated in xylene for 5 min and coverslipped with permount. The slides were kept for at least two months before imaging under the 100X lens of a Nikon Eclipse E800 microscope. Secondary dendritic segments of 30-40 μm length from 4-5 neurons in the CA1 and another 4-5 neurons from the CA3 area from each animal were analyzed for the number of dendritic spines.

Electrophysiology

Electrophysiological experiments were performed using in vitro slice preparation. Mice (pd20-30) were decapitated under halothane anesthesia. The brain was removed immediately and placed in ice cold, oxygenated (95% O_2/5% CO_2) artificial cerebrospinal fluid

(aCSF) containing (in mM): 125 NaCl, 3.5 KCl, 26 $NaHCO_3$, 1 $MgCl_2$ and 10 glucose (pH = 7.4, 315 mOsm/l). The brain part containing the hippocampus was blocked and glued onto the stage of a vibratome (Leica, VT1000S, Leica Biosystems GmbH, Wetzlar, Germany). 400 μm thick brain slices containing the hippocampus were taken and transferred to a submerged chamber, which was continuously superfused with oxygenated (95% O2/5% CO2) aCSF containing (mM): 125 NaCl, 3.5 KCl, 26 $NaHCO_3$, 2 $CaCl_2$, 1 $MgCl_2$ and 10 glucose (pH = 7.4, 315mOsm/l) in room temperature (namely control aCSF). The slices were incubated for 6 hr in one of the following conditions (n = 6): control aCSF, or the selective autophagy inhibitor (SBI-0206965, 500nM, SIGMA) (Egan et al., 2015), or BDNF antibody (mAb#9, 1:100 dilution of stock, DSHB) or BDNF antibody and autophagy inhibitor. Slices were then transferred to a submerged recording chamber, which continuously superfused oxygenated (95% O2/5% CO2) aCSF containing (in mM): 125 NaCl, 3.5 KCl, 26 $NaHCO_3$, 2 $CaCl_2$, 1 $MgCl_2$ and 10 glucose (pH = 7.4, 315mOsm/l) at room temperature. Extracellular recording electrodes filled with NaCl (2M) were placed in the stratum radiatum (SR) layer of the CA1 region. Platinum/iridium metal microelectrodes (Harvard apparatus UK, Cambridge, UK) were also placed in the SR layer, about 300 μm away from the recording electrode, and were used to evoke fEPSPs. The voltage responses were amplified using a Dagan BVC-700A amplifier (Dagan Corporation, Minneapolis, MN, USA), digitized using the ITC-18 board (Instrutech) on a PC using custom-made procedures in IgorPro (Wavemetrics, Lake Oswego, OR, USA). The electrical stimulus consisted of a single square waveform of 100 μsec duration given at an intensity that generated 40% of the maximum fEPSP, using a stimulator equipped with a stimulus isolation unit (World Precision Instruments). Data were acquired and analyzed using custom-written procedures in IgorPro software (Wavemetrics, Lake Oswego, OR, USA). The voltage response was analyzed in order to measure the fEPSP slope. Baseline responses were monitored for at least 10 min, then three theta-burst trains (5X 4spikes at 100Hz) with an inter-stimulus interval of 20 s were applied and finally responses were acquired for 30 min post-tetanus. The fEPSP slope of each response was normalized to the average 10 min pre-tetanic average fEPSP slope. Statistical analyses were performed by multi-way ANOVA.

Electron Microscopy

Preparation of brain slices for electron microscopy was performed as previously described (Alirezaei et al., 2010; Dalezios et al., 2002), with slight modifications. Briefly, mice were perfused with 0.9% saline followed by 4% paraformaldehyde, 1.5% glutaraldehyde in 0.1 M cacodylate buffer with 1 mM CaCl2. The brains were removed and immersed in the above fixative on ice for 6 hr, and then was transferred to 2.5% glutaraldehyde in 0.1 M cacodylate buffer + 1 mM CaCl2 for overnight fixation and then sectioned with a vibratome (Leica) into 200μm thick sections. Sections were further fixed in 1% OsO4 in 0.1 M Na cacodylate and again washed in cacodylate buffer. Tissue sections were dehydrated in a series of ethanol and propylene oxide and embedded flat in epoxy resin (Durcupan ACM, Fluka, Sigma-Aldrich, Gillingham, UK) on slides. After the polymerization of the resin, selected small pieces of the sections from the CA1 region of the hippocampus were re-embedded in Durcupan blocks for sectioning. Serial 70–80 nm thick sections were collected on pioloform-coated copper grids (Klionsky et al., 2016). Sections were examination on a Jeol JEM-210 electron microscope.

Neuronal Cultures

The hippocampi of embryonic day 17 (E17), derived from mixed sex mouse embryos were dissected (Seo et al., 2011) in PBS containing glucose (0.2%) and BSA (0.1%), treated with 0.5% trypsin for 10 min at 37°C followed by mechanically dissociation. After centrifugation (5 min at 1000 rpm), cells were plated in 12-well plates containing 18-mm glass coverslips, coated overnight with poly-D-lysine (Sigma-Aldrich), and cultured in Neurobasal medium (GIBCO) supplemented with B-27 (2%), L-glutamine (200 μM), penicillin (5 μg/μl), and streptomycin (12.5 μg/μl). The initial density was 125,000cells/cm^2 in a final volume of 1 ml/well. After at least 15-21 days *in vitro*, neurons were treated with recombinant BDNF (50 or 100ng/ml) and with the following inhibitors at the indicated final concentrations: K252a (Cell Signaling, 0.5μM), Xestospongin A (Santa Cruz, 1μM), LY294002 (Cell Signaling, 50μM), U0126 (Cell Signaling, 10μM), PD98059 (Cell signaling, 5μM), Rapamycin (Sigma-Aldrich, 10nM), Bafilomycin A1 (Sigma-Aldrich, 1,5nM). All treatments were performed for a period of 24 hr, unless indicated otherwise, with the exception of Bafilomycin A1 which was applied for 6 hr.

Immunostaining

Cultured neurons were rinsed in PBS and fixed for 15 min in 4% paraformaldehyde (PFA) in PBS. Following fixation, cells were rinsed in PBS and incubated for 1 hr in blocking solution containing 10% horse serum and 0.2% Triton-X in PBS. Neurons were then incubated in blocking solution containing primary antibody for 24 hr at 4°C. PBS was substituted for the primary antibodies to test for unspecific labeling. The following primary antibodies were used: LC3 (1:1000, rabbit polyclonal, Cell Signaling), β-III tubulin (1:2000, mouse monoclonal, Santa Cruz). Neurons were rinsed in PBS and incubated with the following secondary antibodies (Abcam) for 1 hr at room temperature: anti-rabbit Alexa 488, anti-mouse Alexa 594, and anti-guinea pig Alexa 647. The nuclear dye Hoechst was used (1:5000) to stain nuclei. Neurons were rinsed in PBS and mounted onto slides. Confocal images of fluorescently labeled proteins were captured using the LSM 710 NL multi-photon microscope (Zeiss).

Isolation of Autophagosomes from the Brain

Based on the described in detail protocols elsewhere (Strømhaug et al., 1998; Berg et al., 1998; Seglen and Brinchmann, 2010), we developed a method to isolate and purify autophagosomes from hippocampus and cortex of mouse brain. For that purpose ten male B6 mice were sacrificed and 10 cortices and hippocampi were collected in 25ml of 10% (w/v) sucrose, 10mM HEPES and 1mM

EDTA. These parts of brain tissue were homogenized by 20 strokes using a Dounce glass homogenizer and the homogenate was diluted with half volume of homogenization buffer (HB) (250mM sucrose, 10mM HEPES, 1mM EDTA pH 7.3) containing 1.5mM glycyl-L-phenylalanine 2-naphthylamide (GPN) in order to achieve a final GPN concentration of 0.5mM. The material was incubated at 37°C for 7min for the lysosomes to be osmotically disrupted and then cooled at 4°C. From this step everything was done on ice. The homogenate was centrifuged at 2000 g for 2min and the supernatant was collected. The obtained nuclear pellets were washed once in HB bf and were centrifuged again. The supernatants were combined to give the single post nuclear supernatant (PNS). To remove mitochondria and peroxisomes discontinuous Nycodenz gradients were prepared using per gradient 7ml of 22.5% heavy Nycodenz (1,127 g/ml) using HB buffer and 17ml of 9.5% light Nycodenz (1,072 g/ml). The PNS was placed on the top of the gradients in 40ml SW28 tubes (14ml of PNS per gradient) and was centrifuged at 28,000rpm (Sorvall centrifuge) for 1h at 4°C. The interface (APs and endoplasmic reticulum) was isolated and diluted with an equal volume of HB buffer to be loaded on Nycodenz-Percoll gradients in order to remove the small-vesicular and unmembraneous material. The Nycodenz-Percoll gradients were prepared in 40ml SW28 tubes by placing 7ml of 22.5% Nycodenz (1,127 g/ml) using HB buffer at the bottom and 21ml of 33% Percoll in double strength HB buffer at the top. Then the material was centrifuged at 20,000rpm (Sorvall centrifuge) for 30min at 4°C to remove the endoplasmic reticulum, and the interface was collected again. The material was then diluted with 0.7V of 60% buffered Optiprep and the removal of Percoll silica particles followed by placing 8.5ml of the diluted material in SW40 tubes overlayed with 1.5ml of 30% iodixanol and a top layer of 2.5ml of HB buffer. The material was then centrifuged at 20,000 rpm (Sorvall centrifuge) for 30min at 4°C resulting to the sedimented Percoll particles at the bottom of the tube and the autophagosomes band floated to the iodixanol/HB interface. Autophagosomes were collected and diluted with three volumes of HB buffer and mixed gently to a homogeneous suspension. A sample of the purified autophagosomes was used for protein determination, and the material was centrifuged in tubes at 15,000rpm for 10min to be stored as frozen pellets for western blot analysis and carbonate extraction experiments. For carbonate extraction, 100 μg of APs were incubated with freshly prepared 0.1M sodium carbonate for 30min on ice and the material was centrifuged at 20psi for 30min in an airfuge centrifuge. The pellet was collected in Laemmle buffer and the proteins of the supernatant were precipitated using 10% TCA. After 20min incubation on ice, the material was centrifuged at 13,000rpm for 20min and the pellet was washed with 75% ethanol. Pellets were then left to air-dry and resuspended in Laemmle buffer. Both pellets and TCA-precipitated supernatants were in the end boiled at 95C for 5min for western blot analysis.

QUANTIFICATION AND STATISTICAL ANALYSIS

All experiments reported in Figures 1, 2, 3, and 4 were repeated with N = 6 animals per condition or per genotype. For the quantification of autophagosomes and autolysosomes by electron tomography in Figure 4, 20 neurons were analyzed per genotype. Experiments shown in Figures 6 and S1 were repeated with N = 3 animals per genotype. All samples represent biological replicates and N values are indicated in figure legends. No samples or animals were excluded from analysis. Animals were randomly assigned to groups. Behavioral studies of fear conditioning were conducted blinded. Statistical analyses were performed with the GraphPad Prism 4 software, and the data are presented as mean ± SEM. For statistical significance of the differences between the means of two groups, we used two-tailed Student's t tests. Statistical significance of differences among multiple groups (R3) was calculated by performing ANOVA multiple comparisons of the means for each group.